Testing and developing an instrumented microlysimeter for automated estimation of *in situ* soil evaporation

by

Sofia Cominelli

B.S., Universidad Nacional de Rosario, 2019

A THESIS

submitted in partial fulfillment of the requirements for the degree

MASTER OF SCIENCE

Department of Agronomy
College of Agriculture

KANSAS STATE UNIVERSITY
Manhattan, Kansas

2024

Approved by:

Major Professor
Andres Patrignani

Copyright

© Sofia Cominelli 2024.

Abstract

In rainfed cropping systems of the U.S. Great Plains, precipitation represents the main input and evapotranspiration, runoff, and drainage represent the main outputs of the soil water balance. In the state of Kansas, about 87% of the annual precipitation returns to the atmosphere through the evapotranspiration process, where unproductive soil evaporative losses can account for 30% to 50% of total evapotranspiration. Given this context, it is essential to identify and assess new crop rotations and agronomic practices aimed at shifting non-productive evaporative losses into productive transpirational losses. Commonly, soil evaporation is measured using the microlysimeter technique, but this technique is labor intensive and only suitable for short periods. Since soil evaporation rate depends on surface soil moisture conditions, this thesis is centered around a pivotal question: *Can we use soil moisture observations from electromagnetic sensors to accurately estimate in situ soil evaporation through a data-driven approach?* The first chapter of this thesis explores the accuracy of two new electromagnetic sensors, the TEROS 10 and TEROS 12, in sand, loam, and silty clay loam soils at various moisture levels. The second chapter introduces five different data-driven approaches that combine the FAO-56 Dual Crop Coefficient model with 1) *in situ* observations from a calibrated soil moisture sensor and 2) measurements of green canopy cover to quantify soil evaporation rates in winter wheat and bare soil. Overall, the results of our study demonstrate the feasibility of using a simple model coupled with *in situ* soil moisture observations to estimate soil evaporation rates during the entire growing season.

Table of Contents

List of Figures

List of Tables

Acknowledgements

I would like to acknowledge my family and friends for their unconditional love and support. I also want to thank my main advisor for guiding and mentoring me throughout my research journey, encouraging my professional growth and critical thinking. I also want to acknowledge the support and feedback that I received from my committee members, Dr. Gerard Kluitenberg and Dr. Eduardo Santos. Additionally, I am grateful to my fellow graduate students for their consistent support, both academically and personal.

Chapter 1 - General Introduction

The soil water balance represents the inflow and outflow of water on the land surface, where precipitation is the main inflow in rainfed systems and soil evaporation (E), plant transpiration, canopy interception, surface and sub-surface runoff, and drainage are the main outflows that shape the hydrological budget of a region (Hillel, 2012; Wilcox et al., 2003). Globally, ~65% of the water that falls on the Earth's surface returns to the atmosphere through the combined process of evapotranspiration (ET), while the remaining 35% mostly represents losses due to runoff and drainage (Rodell et al., 2011; Trenberth et al., 2007). On average, the state of Kansas receives 685 mm of precipitation per year, where approximately 85-90% of this precipitation returns to the atmosphere through ET (Reitz et al., 2017; Sophocleous, 1998). Given the prevalence of ET as the primary outflow component in the soil water balance of this region, and the inherent difficulties in separately measuring soil evaporation, canopy interception, and plant transpiration, scientists have historically focused on quantifying the combined ET process. At the fundamental level, the process of soil evaporation, canopy interception, and plant transpiration are essentially an evaporative process (i.e., phase change from liquid to vapor). Nonetheless, plant transpiration is a process tightly linked to primary biomass production, while evaporation from the soil surface and leaf or residue surfaces can be considered unproductive water losses. Thus, understanding the magnitude of soil evaporative losses is essential to develop, identify, and assess crop rotations and tactical agronomic management practices that could shift non-productive evaporative losses into productive evaporative losses.

In the U.S. southern and central Great Plains (Texas, Oklahoma, Kansas, eastern Colorado), hard red winter wheat (*Triticum aestivum* L.) is the predominant crop with a total

annual production that exceeds 20 million metric tons, which represents ~30% of the entire wheat production for the United States (Lollato et al., 2017; USDA-NASS, 2016). The state of Kansas is one of the largest producers of winter wheat in the U.S. with an estimated planting area of 2.8 to 3.6 million hectares per year and grain yields averaging about 2,700 kg ha^{-1} (Holman et al., 2011; Jaenisch and Lollato, 2019). However, winter wheat systems in this region exhibit clear signs of yield stagnation and poor use of available precipitation, where about 60-70% of the annual precipitation in wheat-dominated cropping systems can be lost in the form of unproductive evaporative losses (Patrignani et al., 2014; Warren et al., 2009).

Crop evapotranspiration measurements have traditionally been measured using field lysimeters (Howell et al., 1985; Putz et al., 2018), which have played a central role in validating other methodologies based on soil moisture sensors, eddy covariance towers, and Bowen ratio systems (Evett et al., 2016). Field lysimeters typically consist of a large volume (i.e., one to several cubic meters) containing undisturbed soil and are equipped with accurate weighing load cells to precisely measure hydraulic fluxes like rainfall, drainage, and ET (Singh et al., 2018). However, in order to measure soil evaporation separately during the growing season, researchers need to make use of other methodologies. A simple and common method for accurately measuring evaporation rate with minimal equipment is to use the microlysimeter technique. This technique is well suited for measuring soil evaporation rate in conditions where micrometeorological and traditional lysimeter methods are impractical or impossible to use, such as measuring soil evaporation in small experimental plots without enough fetch for micrometeorological methods or surface area for installing lysimeters. The microlysimeter technique has an accuracy <0.1 mm day^{-1} (Klocke et al., 1990) and a relative error of about 7% (Boast and Robertson, 1982), thus, this method is often considered the "gold standard" for *in situ*

measurements of evaporation. The microlysimeter technique is based on the assumption that, over short time intervals, disruptions to the lower boundary conditions (e.g., sealing) has a negligible impact on the rate of soil evaporation. The first study describing and testing the use of the microlysimeter technique was a laboratory experiment that measured the soil evaporation rate in a silty clay loam soil collected at the University of Illinois Agronomy Farm (Boast and Robertson, 1982). Subsequent studies have used the microlysimeter technique to measure evaporation in a wide range of scenarios. For instance, Villalobos and Fereres (1990) used the microlysimeter technique to study ET partitioning in irrigated corn (*Zea mays* L.), cotton (*Gossypium hirsutum* L.), and sunflower (*Helianthus annuus* L.) fields in southern Spain. Flumignan et al. (2012) used microlysimeters to measure evaporation rate in bare soil under both irrigated and non-irrigated conditions in Brazil. Zhao et al. (2018) quantified ET partitioning in a vineyard with sandy loam soils in northwest China. Rafi et al. (2019) quantifies evaporative losses of drip-irrigated wheat in Morocco and da Rocha et al. (2022) used microlysimeters to validate ET partitioning by eddy covariance flux measurements in a tallgrass prairie in Kansas.

Two critical aspects for the successful implementation of the microlysimeter method are its length and wall material. The length of the microlysimeter exerts a strong control on the amount of water that can be supplied to the evaporating surface during the measurement period. Studies investigating the effects of microlysimeter length on soil evaporation accuracy suggest that a length of 10 to 15 cm is often adequate for short measurement periods (i.e., 2-3 days), while a length of 30 cm is often required for periods of up to nine consecutive days (Daamen et al., 1993; Evett et al., 1995). On the other hand, the microlysimeter material has important implications for heat transfer. Studies dedicated to examining microlysimeter wall materials, such as polyvinyl chloride (PVC) and steel, concluded that using less thermally conductive

materials, like PVC, closely match the thermal conductivity of mineral soils (Evett et al., 1995). In the same study, the researchers concluded that using a thin plastic or nylon material are the best choice for capping the bottom of the microlysimeter and minimizing disruption of heat flow from deeper soil layers. These studies show that readily available and inexpensive supplies from hardware stores could be used to accurately measure soil evaporation in a wide range of scenarios.

Nonetheless, microlysimeters have some well-known limitations, which mainly include the small measurement area, the amount of labor required to install and periodically weigh the microlysimeters, and the fact that soil moisture conditions within the microlysimeter volume start to diverge from that of the surrounding soil after a few days due to differential root water uptake and restricted capillary flow. To overcome some of these limitations, scientists have used long (e.g., 80 cm) columns filled with undisturbed soil on top of automated load cells (Rumana, 2015) and microlysimeters paired with soil moisture sensors for continuous monitoring of soil evaporation rate based on changes in soil water storage (Baker & Spaans, 1994). The experiment conducted by Baker & Spaans (1994) in Minnesota that consisted of 20-cm long microlysimeters filled with soil, sealed at the bottom with drainage perforations, and equipped with time domain reflectometry waveguides demonstrated good agreement with independent soil evaporation measurements obtained using a Bowen ratio system (Baker & Spaans, 1994). Two common disadvantages associated with microlysimeters using either load cells or soil moisture sensors inserted from the bottom are 1) the need for excavation and 2) the need for sealing the bottom of the microlysimeter, which sooner or later, would result in differences in soil moisture levels between the microlysimeter and the surrounding soil.

Based on these previous attempts to automate soil evaporation measurements, we propose to develop and test an open-bottom microlysimeter instrumented with a soil moisture sensor and assimilate these observations of surface soil water storage into a simple evaporation model. The first part of this thesis focuses on the determination of the sensing volume and the calibration of electromagnetic sensors using different mineral soils. The second chapter describes the development and testing of a model-data assimilation approach that combines a simple evaporation model with surface soil moisture observations. The second chapter also explores the assimilation of the fraction of green canopy cover, with the goal of testing whether measuring variables that regulate the partition of energy or the supply of water have a more prominent impact on the modeling of soil evaporation rate.

References

Baker, J. M., & Spaans, G. J. (1994). Measuring water exchange between soil and atmosphere with TDR-microlysimetry. *Soil science, 158*(1), 22-30. https://doi.org/10.1097/00010694-199407000-00003

Boast, C. W., & Robertson, T. M. (1982). A "Micro-Lysimeter" method for determining evaporation from bare soil: Description and laboratory evaluation. *Soil Science Society of America Journal*, *46*(4), 689-696. https://doi.org/10.2136/sssaj1982.03615995004600040005x

Da Rocha, A. E. Q., Santos, E. A., & Patrignani, A. (2022). Partitioning evapotranspiration in a tallgrass prairie using micrometeorological and water use efficiency approaches under contrasting rainfall regimes. *Journal of Hydrology*, *608*, 127624. https://doi.org/10.1016/j.jhydrol.2022.127624

Evett, S. R., Warrick, A. W., & Matthias, A. D. (1995). Wall material and capping effects on microlysimeter temperatures and evaporation. *Soil Science Society of America Journal*, *59*(2), 329-336. https://doi.org/10.2136/sssaj1995.03615995005900020009x

Evett, S. R., Howell, T. A., Schneider, A. D., Copeland, K. S., Dusek, D. A., Brauer, D. K., ... & Gowda, P. H. (2016). The Bushland weighing lysimeters: A quarter century of crop ET investigations to advance sustainable irrigation. *Transactions of the ASABE,* 59(1), 163-179. https://doi.org/10.13031/trans.59.11159

Flumignan, D. L., Faria, R. T. D., & Lena, B. P. (2012). Test of a microlysimeter for measurement of soil evaporation. *Engenharia Agrícola*, 32, 80-90, https://doi.org/10.1590/S0100-69162012000100009

Hillel, D. (2012). Soil and water: Physical principles and processes. *Elsevier*.

Holman, J. D., Schlegel, A. J., Thompson, C. R., & Lingenfelser, J. E. (2011). Influence of precipitation, temperature, and 56 years on winter wheat yields in Western Kansas. *Crop Management*, *10*(1), 1-10. https://doi.org/10.1094/CM-2011-1229-01-RS

Howell, T. A., McCormick, R. L., & Phene, C. J. (1985). Design and installation of large weighing lysimeters. *Transactions of the ASAE*, 28(1), 106-0112. https://doi.org/10.13031/2013.32212

Jaenisch, B. R. and Lollato, R. P. (2019). Integrated wheat Management for Improved Wheat Yield and Protein in Kansas. *Kansas Agricultural Experiment Station Research Reports*: Vol. 5: Iss. 6. https://doi.org/10.4148/2378-5977.7786

Klocke, N. L., Todd, R. W., & Schneekloth, J. P. (1996). Soil water evaporation in irrigated corn. *Applied Engineering in Agriculture*, 12(3), 301-306., doi: 10.13031/2013.25652

Lollato, R. P., Edwards, J. T., & Ochsner, T. E. (2017). Meteorological limits to winter wheat productivity in the U.S. Southern Great Plains. *Field Crops Research*, *203*, 212-226. https://doi.org/10.1016/j.fcr.2016.12.014

Patrignani, A., Lollato, R. P., Ochsner, T. E., Godsey, C. B., & Edwards, J. T. (2014). Yield gap and production gap of rainfed winter wheat in the Southern Great Plains. *Agronomy Journal*, *106*(4), 1329-1339. https://doi.org/10.2134/agronj14.0011

Pütz, T., Fank, J., & Flury, M. (2018). Lysimeters in vadose zone research. *Vadose Zone Journal*, *17*(1), 1-4. https://doi.org/10.2136/vzj2018.02.0035

Rafi, Z., Merlin, O., Le Dantec, V., Khabba, S., Mordelet, P., Er-Raki, S., Amazirh, A., Olivera-Guerra, L., Ait Hssaine, B., Simonneaux, V., Ezzahar, J., & Ferrer, F. (2019). Partitioning evapotranspiration of a drip-irrigated wheat crop: Inter-comparing eddy covariance-, sap

flow-, lysimeter- and FAO-based methods. *Agricultural and Forest Meteorology*, *265*, 310-326. https://doi.org/10.1016/j.agrformet.2018.11.031

Reitz, M., Sanford, W. E., Senay, G. B., & Cazenas, J. (2017). Annual estimates of recharge, quick-flow runoff, and evapotranspiration for the contiguous U.S. using empirical regression equations. *Journal of the American Water Resources Association*, *53*(4), 961-983. https://doi.org/10.1111/1752-1688.12546

Rodell, M., McWilliams, E. B., Famiglietti, J. S., Beaudoing, H. K., & Nigro, J. (2011). Estimating evapotranspiration using an observation based terrestrial water budget. *Hydrological Processes*, *25*(26), 4082-4092. https://doi.org/10.1002/hyp.8369

Rumana, K. (2015). Novel techniques to determine soil evaporation rates: heat pulse probe and automated microlysimeter.

Singh, G., Kaur, G., Williard, K., Schoonover, J., & Kang, J. (2018). Monitoring of water and solute transport in the vadose zone: a review. *Vadose Zone Journal*, *17*(1), 1-23. https://doi.org/10.2136/vzj2016.07.0058

Sophocleous, M. (1998). Perspectives on sustainable development of water resources in Kansas (Vol. 239). *Kansas Geological Survey*.

Uclés, O., Villagarcía, L., Cantón, Y., & Domingo, F. (2013). Microlysimeter station for long term non-rainfall water input and evaporation studies. *Agricultural and Forest Meteorology*, *182-183*, 13-20. https://doi.org/10.1016/j.agrformet.2013.07.017

USDA-NASS, 2016. United States Department of Agriculture—National Agricultural Statistics Service Cropland Data Layer. Published Crop-specific Data Layer for the 2015 Season [online], Available at: http://datagateway.nrcs. usda.gov/gdghome statusmaps.aspx

Villalobos, F. J., & Fereres, E. (1990). Evaporation measurements beneath corn, cotton, and sunflower canopies. *Agronomy Journal*, *82*(6), 1153-1159. https://doi.org/10.2134/agronj1990.00021962008200060026x

Warren, J. G., Ochsner, T. E., & Godsey, C. B. (2009). Fate of precipitation falling on Oklahoma cropland. *Oklahoma Cooperative Extension Service*.

Wilcox, B. P., Seyfried, M. S., Breshears, D. D., Stewart, B., & Howell, T. (2003). The water balance on rangelands. *Encyclopedia of water science*, 791(4). 10.1081/E-EWS 120010097

Zhao, P., Kang, S., Li, S., Ding, R., Tong, L., & Du, T. (2018). Seasonal variations in vineyard ET partitioning and dual crop coefficients correlate with canopy development and surface soil moisture. *Agricultural Water Management*, 197, 19-33. https://doi.org/10.1016/j.agwat.2017.11.004

Chapter 2 - Calibration of TEROS 10 and TEROS 12 Electromagnetic Soil Moisture Sensors

Abstract

Electromagnetic soil moisture sensors rely on calibration equations to convert measurements of soil dielectric properties into volumetric soil water content. However, this relationship is often susceptible to the effect of soil temperature and bulk electrical conductivity, hindering accurate soil moisture measurements across multiple soils. Thus, research applications often demand verifying the accuracy of factory default equations. The objectives of this study were to: 1) calibrate the TEROS 10 and TEROS 12 capacitance soil moisture sensors, and 2) determine the sensing volume of each sensor in minerals soils. Calibration equations were determined in the laboratory using columns of packed sand, loam, and silty clay loam soils. For each soil type, the process involved sieving, oven-drying, and homogenizing the soils with six different levels of soil moisture 0, 0.05, 0.15, 0.25, 0.35, and 0.45 cm^3 cm^{-3}. The sensing volume was determined by quantifying the response of raw sensor outputs while increasing the level of oven-dry sand and moist sand (0.100 cm^3 cm^{-3}) around the sensor in the radial and axial directions. The sensing volume was assumed to be elliptical in shape. For the TEROS 10, a cubic polynomial with factory-default parameters resulted in a root mean square error (RMSE) of 0.027 cm^3 cm^{-3}. The same model with fitted parameters using the three soils and six soil moisture levels resulted in improved accuracy with a RMSE of 0.017 cm^3 cm^{-3}. For the TEROS 12 sensor, the manufacturer's recommended linear equation resulted in a RMSE of 0.037 cm^3 cm^{-3} and the same model with fitted parameters had a RMSE of 0.035 cm^3 cm^{-3}. A cubic polynomial equation with fitted parameters was required for the TEROS 12 to reach more accurate soil moisture

estimation with a RMSE of 0.025 cm^3 cm^{-3}. The resulting mean sensing volume of the TEROS 10 was 280 cm^3 and for the TEROS 12 was 415 cm^3.

Introduction

Soil water content is an essential climate variable (Hollmann et al., 2013; Bojinski et al., 2014) that plays a vital role in vadose zone hydrology and agriculture by controlling the partitioning of energy and water fluxes. For instance, soil moisture is one of the drivers controlling the partitioning of net solar radiation into sensible, latent, and soil heat fluxes (Cavanaugh et al., 2011; Rigden et al., 2018; Scanlon and Kustas, 2012; Scott et al., 2021) and the partitioning of precipitation into infiltration and surface runoff (Kiekby, 1988; Rockström et al., 1998). Thus, accurate soil moisture measurements are essential for understanding and quantifying processes of the surface energy balance and the soil water balance. From an agronomic perspective, soil moisture has a direct impact on crop yield and productivity (Holzman et al., 2014), particularly in rainfed systems, in which rootzone soil moisture can provide valuable information to guide in-season management decisions like defining the planting date of winter wheat (*Triticum aestivum* L.) (Lollato et al., 2016), the timing and amount of in-season nitrogen fertilizer application (Bushong et al., 2016; Walsh et al., 2013; Zotarelli et al., 2009), and the potential onset of crop diseases such as powdery mildew (*Blumeria graminis)* and anthracnose (*Colletotrichum graminicola*) (Kumar et al., 2020; Patle et al., 2021). In irrigated systems, information about rootzone soil moisture conditions is critical for improving both the timing and amount of water applications (Fares and Alva, 2000; Hanson et al., 2000; Irmak et al., 2000).

Soil moisture sensors based on electromagnetic principles, such as time and frequency domain reflectometry, time domain transmissometry, capacitance, and radio-frequency spectroscopy dominate the market of consumer-grade and research-grade sensors due to the their cost-effectiveness, seamless integration with dataloggers, user-friendly operation, capacity for

temporal resolutions from minutes to hours or daily intervals, and the capability to monitor soil water content at different depths, employ data telemetry systems, and facilitate simultaneous measurements of soil moisture, soil temperature, and bulk electrical conductivity. Electromagnetic sensors work by measuring the soil's apparent dielectric permittivity (K_a), which represents a material's ability to store electric charge through the polarization and rearrangement of its molecules when subjected to an electric field created by applying a voltage difference across the material. The dielectric permittivity of soil components is often expressed relative to that of vacuum (8.854×10^{-12} F m^{-1}). Water, with its high dielectric constant (K_a ~78 at 20 ℃), stands in contrast to other soil components such as air (K_a ~ 1) and soil solids (K_a 2-5), making the determination of the relative permittivity an effective method for measuring water content in porous media (Topp et al., 1980; Topp and Reynolds, 1998).

Electromagnetic soil moisture sensors have been widely used to characterize soil moisture spatial variability at the catchment scale (Brocca et al., 2007; Walker et al., 2001; Western and Grayson 1998), to incorporate soil moisture conditions into model-based rainfall-runoff partitioning (Aubert et al., 2003; Tramblay et al., 2010), asses drought conditions (Ford et al., 2015; Ford et al., 2019; Krueger et al., 2019), understand the role of soil moisture as an indicator of growing season herbaceous fuel moisture and curing rate in grasslands (Sharma et al., 2021), develop sensor-based irrigation scheduling (Martínez-Gimeno et al., 2020; Ortega-Farias & Acevedo, 2004), delineate soil moisture-based management zones in agricultural fields (Rossini et al., 2021), measure soil evaporation rate using instrumented microlysimeters (Baker & Spaans, 1994), and to study soil moisture controls on ET partitioning (Cavanaugh et al., 2011; Ding et al., 2013; Zhao et al., 2018).

The TEROS sensor series (METER Group, Inc.) is a new family of electromagnetic soil moisture sensors that offer a practical and cost-effective alternative for *in situ* monitoring without the need for expensive pulse and sampling units required by traditional time domain reflectometry sensors. Sensors from the TEROS family have been employed in diverse scientific studies, including research on irrigation scheduling of drip-irrigated tomatoes (*Solanum lycopersicum* L.) (Bwambale et al., 2023), the assessment of sensitivity in apple trees (*Malus domestica*. L) of variations in soil water status within orchard systems (Mohamed et al., 2021), and the monitoring of root zone soil water storage in a watershed dominated by a tallgrass prairie (Patrignani et al., 2022), as well as in the validation of soil moisture measurements using cosmic-ray neutron sensors (Flynn et al., 2021).

Since electromagnetic soil moisture sensors measure the dielectric properties of the soil, a calibration equation is often required to convert raw sensor outputs that are related to the soil's relative permittivity into volumetric soil water content. Sensor manufacturers usually adopt either a third-order polynomial, first proposed in the seminal work of Topp et al. (1980) for time domain reflectometry (TDR) sensors, or a custom equation based on factory calibrations, but some of these equations have shown large errors, particularly in fine-textured soils with high bulk electrical conductivity (Ojo et al., 2015; Cosh et al., 2016). Thus, for research applications, the accuracy of the factory default equation usually needs to be verified with the soil under study, and if necessary, researchers need to develop customized calibration equations to ensure adequate levels of accuracy. Similarly, the sensing volume of electromagnetic soil moisture sensors can vary widely depending on the selected sensor response stopping criterion and media used for determining the maximum sensing volume (Patrignani et al., 2021). Since the TEROS sensors use a high-frequency oscillating wave, which minimizes textural and salinity effects, and

are factory calibrated using a wide range of soils (personal communication with Meter TEROS developing team), we hypothesize that the generic factory calibration equation for each TEROS sensor that converts raw sensor outputs into volumetric soil water content applies to multiple soil textures from oven-dry to saturation conditions with a root mean square error (RMSE) <0.03 cm^3 cm^{-3}, which is a reasonable benchmark for most practical field applications in agriculture and hydrology. Also, accurate determination of the sensing volume of soil moisture sensors is essential to guide the installation depth, sensor orientation, and sensor spacing along the soil profile. The objectives of this study were to: 1) calibrate the TEROS 10 and TEROS 12 soil moisture sensors under laboratory conditions and 2) determine the sensor sensing volume in mineral soils.

Materials and Methods

Sensors description

The TEROS sensor series uses a 70-MHz oscillating wave to measure the K_a of porous media. When an electromagnetic field is applied to a dielectric material like soil, the electric charges inside the soil particles and pore water rearrange themselves in response to the electric field created by a voltage differential. The redistribution and storage of electrical charge between two electrodes or sensor rods (i.e., capacitance) results in a raw voltage output ranging from 1,000 to 2,500 mV. This voltage output is then converted into volumetric soil water content (VWC) using an empirical calibration equation. In this study we used the TEROS 10 and TEROS 12 sensors, which represent the most basic and most advanced sensors of the TEROS sensor series, respectively.

The TEROS 10 sensor consists of an epoxy-filled head with two sharp stainless-steel rods that have a length of 5.4 cm. The TEROS 10 is the simplest and most affordable sensor of the TEROS family and only measures VWC. The TEROS 12 sensor has an epoxy-filled head with three stainless steel rods that are 5.5 cm in length arranged in a linear array. In addition to VWC, the TEROS 12 sensor also measures soil temperature with a thermistor embedded in the central rod and bulk electrical conductivity (EC_b) between needles 2 and 3 (Figure 2-1). In the case of the TEROS 12, the 70 MHz signal is applied to needle 1, and needle 2 and needle 3 are used as the reference for the soil moisture measurement.

Laboratory calibration procedure

The sensors were calibrated using columns of uniformly sieved and packed sand (sand = 100%, clay = 0%), loam (sand = 42%, clay = 13%), and silty clay loam (sand = 10%, clay = 28%) soils (Table 2-1). The soils were oven dried at 105 °C, ground (except for sand), and sieved to pass a 2 mm mesh. Then, the soil was thoroughly mixed with known amounts of water to reach nominal moisture levels of 0, 0.05, 0.15, 0.25, 0.35, and 0.45 VWC. The soils were carefully packed into cylindrical containers with a diameter of 18 cm, a height of 16 cm, and a total volume of 4,072 cm^3. The soils were packed in four layers of 4 cm each to minimize variations in bulk density along the length of the soil columns. Each layer was packed to a target bulk density of 1.6 g cm^{-3} for sand and 1.2 g cm^{-3} for the loamy sand and silty clay soils. Particle size was determined using the hydrometer method (Gavlak et al., 2005)

After packing the soil columns, the TEROS 10 and TEROS 12 sensors were inserted in the center of the filled container with the sensor rods pointing downwards while maintaining a distance of 4 cm from the bottom of the bucket to minimize signal loss. The sensor head was

covered with soil (Appendix A Figure A- 1). Sensor voltage output values and VWC were recorded with a datalogger (model CR300, Campbell Scientific, Inc.). After collecting the sensor readings, one undisturbed soil sample with a volume of 100 cm^3 was collected from the center of each container for determination of the actual VWC using the thermo-gravimetric method, which consisted of oven drying the samples for 48 hours at 105 ˚C. The resulting bulk density was computed as the ratio between the mass of oven-dry soil and the volume of the soil sample (Table 2-1). Raw sensor readings and the observed VWC collected for each soil column were used to verify the factory default equation and fit a sensor-specific calibration equation considering all soils (i.e., universal equation). For the TEROS 10 sensor we used a cubic polynomial (TEROS 10 Manual, 2023) and for the TEROS 12 sensor we used a linear model (TEROS 12 Manual, 2023) according to the manufacturer's manuals. The raw output voltage of each sensor was the predictor variable and the observed VWC was the response variable. The goodness of fit of the calibration models was quantified using the root mean squared error (RMSE), the coefficient of determination (R^2), and the mean absolute error (MAE).

Calibration models

The TEROS 10 sensor converts raw sensor output into VWC using a cubic polynomial model:

$$VWC = a\,Voltage^3 - b\,Voltage^2 + c\,Voltage + d \qquad [2.1]$$

where *Voltage* is the raw output voltage (mV, integer value), and *a*, *b*, *c*, and *d* are fitting parameters. The factory default equation has values of $a = 4.824\text{x}10^{-10}$, $b = -2.278\text{x}10^{-6}$, $c = 3.899\text{x}10^{-3}$, and $d = 2.5154$. On the other hand, the TEROS 12 sensor relies on a linear calibration model:

$$VWC = a - b\,Voltage \qquad [2.2]$$

where a and b are fitting parameters that for the factory calibration equation have values of a = 3.879×10^{-4} and b = -0.6956.

Determination of sensing volume

The sensing volume of the TEROS 10 and TEROS 12 sensors was determined by recording the sensor response in terms of the raw voltage output while gradually varying the level of porous medium surrounding the sensor in the radial and axial directions. Given the form factor and arrangement of the sensor rods, the sensing volume was assumed to have the shape of an elliptical cylinder:

$$V = \pi\, M\, m\, h \qquad [2.3]$$

where V is the sensing volume (cm^3), M is the semi-major radial axis (cm), m is the semi-minor radial axis (cm), and h is the length of the response (cm) (Figure 2-1). To determine the semi-major and semi-minor radial axes of the elliptical cylinder we conducted experiments where the sensor was suspended in three different positions at the center of cylindrical containers with a diameter of 27 cm, a height of 36 cm, and a total volume of 20,612 cm^3 (Figure 2-2). Dry (i.e., 0% VWC) or moist (i.e., 10% VWC) sand was gradually added to the container while the sensor was suspended using a three-fingered laboratory clamp attached to a transversal cross-arm above the container. Sand levels were measured using a laser distance measurer (Bosch Professional GLM 30 model, Bosch Inc.) with an resolution of 1.58 mm. The addition of sand layers ceased when three consecutive readings exhibited the same voltage output (e.g., Patrignani et al., 2022). The computation of the sensing length followed a similar procedure, with the sensor rods pointing upwards and downward (Figure 2-2D and 2-2E). An exponential rise function was used

to approximate the voltage response as a function of the distance from a reference point (e.g., Patrignani et al., 2022):

$$Voltage = \max\{a[1 - b\ exp(-cx)], Voltage_{min}\} \qquad [2.4]$$

where *x* represents the distance from the center according to the sensor orientation, $Voltage_{min}$ is the lowest raw output of the sensor in air, and *a*, *b*, and *c* are fitting parameters. The fitting parameter *a* represents the asymptote of the response. Parameter *a* is the asymptote when the support volume is entirely encompassed within the medium. In this fitting exercise, the value of *a* was not optimized, and instead it was forced to adopt the asymptotic value observed as the maximum raw voltage output. Then, the sensing volume was estimated based on the distance at which the raw sensor response in terms of voltage reached 95% of the asymptotic value of the response for each sensor orientation.

Results and Discussion

Calibration models

During the laboratory calibration of each sensor, linear and polynomial equations were tested to estimate the volumetric water content of mineral soils (Table 2-2). The factory default third-order polynomial calibration equation for the TEROS 10 resulted in a RMSE = 0.027 cm^3 cm^{-3} and R^2 = 0.97, while the same calibration equation with fitted parameters resulted in RMSE = 0.017 cm^3 cm^{-3} and R^2 = 0.99, which represents an improvement in the sensor accuracy of 37% across the sand, loam, and silty clay loam soils tested in this study (Table 2-2, Figure 2-3). For the TEROS 12, the linear equation with factory default parameters had a RMSE = 0.037 cm^3 cm^{-3} and R^2 = 0.94, and the same linear model with fitted parameters resulted in RMSE = 0.035 cm^3 cm^{-3} and R^2 = 0.94, which represents an improvement of only 5% compared to the factory

equation (Table 2-2, Figure 2-3). As a result, both the manufacturer and lab-determined calibration equations for the TEROS 10 sensor resulted in RSME <0.03 cm^3 cm^{-3}, and thus, we accept our initial hypothesis that the TEROS 10 provides accurate volumetric water content readings using the factory default settings. On the other hand, the linear calibration models used in the TEROS 12 sensor exhibited RMSE values >0.03 cm^3 cm^{-3} regardless of whether we used factory default parameters or fitted parameters. In an attempt to seek greater accuracy for the TEROS 12, we also fitted a third-order polynomial calibration, in similar fashion as the model for the TEROS 10 and the model proposed by Topp et al. (1980) for time-domain reflectometry sensors. The third-order polynomial with fitted parameters resulted in RMSE = 0.025 cm^3 cm^{-3} and R^2 = 0.97 (Table 2-2), enhancing soil moisture estimation by 32% compared to the RMSE obtained using the manufacturer's equation (Figure 2-3). Hence, we reject the hypothesis that the TEROS 12 sensor provides accurate volumetric water content readings using the factory default linear model, and we recommend using a third-order polynomial with parameters fitted using a laboratory calibration for greater accuracy.

Several studies have evaluated the accuracy of different soil moisture sensors and our results indicate that the TEROS family of soil moisture sensors offers reliable estimation of soil moisture when compared with RMSE values from prior research studies. For instance, Kizito et al. (2008) assessed the accuracy of the ECH2O sensor, which also works at a frequency of 70 MHz, and found RMSE = 0.02 cm^3 cm^{-3} when using a single calibration curve in sand and loam soils with salinity levels ranging about 1-12 dS m^{-1}. In a laboratory calibration for a time domain reflectometry sensor, Ledieu et al. (1986) obtained a RMSE = 0.038 cm^3 cm^{-3} using a loam soil with varying bulk densities (1.38 and 1.78 g cm^{-1}). In another sensor calibration study, Schaap et al. (1997) achieved an RMSE of 0.036 cm^3 cm^{-3} across five different organic forest soils using a

three-parameter model. Several studies evaluating the CS655 (Campbell Scientific, Inc.) soil water reflectometers demonstrated consistent performance with average RMSE <0.04 cm^3 cm^{-3} across a wide range of soil textural classes (Kargas and Soulis 2019; Patrignani et al., 2022). Vaz et al. (2013) tested eight electromagnetic sensors in seven different soil types ranging from non-saline sandy to clayey soils and obtained RMSE = 0.015 cm^3 cm^{-3} for the 10HS, SM300, and Theta Probe sensors, whereas lower accuracies of about 0.025 cm^3 cm^{-3} were estimated for the TDR100, CS616, Wet2, 5TE, and the Hydra Probe sensors. Other studies have also focused on assessing the error of multi-depth profile sensors. For instance, Geesing et al. (2004) calibrated the Diviner 2000 (Sentek, Inc.), using silty loam and loam soils in Germany and obtained an RMSE of 0.030 cm^3 cm^{-3} when using a linear regression model. Using a non-linear model, Evett et al. (2006) found a superior calibration accuracy for the Diviner 2000 with a RMSE ranging from 0.018 to 0.025 cm^3 cm^{-3} for silty clay loam, clay loam, and clay soils. Polyakov et al. (2005) achieved RMSE values for the EasyAg 50 (Sentek, Inc.) ranging between 0.024 cm^3 cm^{-3} in sand columns and 0.048 cm^3 cm^{-3} in a cultivated silty clay loam soil.

Given that the dielectric permittivity of the soil components, especially water, is influenced by temperature, it is crucial to control and document the soil temperature in the calibration of soil moisture sensors. The temperature range during the calibration ranged from 20.5 ℃ to 25.9 ℃, with an average temperature of 23 ℃ (Figure 2-4). While our calibration did not specifically explore the impact of temperature, it is well known that temperature can affect the dielectric permittivity of soils due to two opposing factors: 1) the relative permittivity of liquid water decreases with increasing temperature, and 2) in low soil moisture conditions, the relative permittivity of water molecules closely bounded to solid surfaces, particularly in high-surface clay minerals, tends to increase with temperature (Jones et al., 2002; Or and Wraith

1999; Wraith and Or, 1999; Patrignani et al., 2022). These opposing phenomena can impact the accuracy of soil moisture estimation in fine-textured soils and uncertainties can propagate into evaporation and infiltration estimates relying on near-surface soil measurements (Jones et al., 2002).

Determination of sensing volume

The sensing volume was estimated by analyzing the sensor voltage response of the TEROS 10 (Figure 2-5) and TEROS 12 (Figure 2-6) during the addition of increasing layers of dry and moist sand (Table 2-3). For the TEROS 10, the semi-major radial axis determined by averaging the distance responses with sensor configurations vertical-cable upwards and vertical-cable downwards resulted in 3.35 cm. The semi-minor radial axis, estimated with the orientation of rods in a horizontal position, was 1.5 cm. The length of the response extending beyond the rods and beyond the sensor head was equal to 8.3 cm, which was obtained by summing the results from the orientation of rods upwards and rods downwards. According to these measurements the sensing volume for the TEROS 10 in dry sand assuming the shape of an elliptical cylinder was 131 cm^3. The same analysis was implemented to determine the sensing volume in moist sand, where the semi-major radial axis resulted in 4.95 cm, the semi-minor radial axis resulted in 3.1 cm, and the overall length of the response was 9.2 cm. Consequently, the sensing volume for the TEROS 10 in moist sand was 444 cm^3, a value similar to the reported value by the manufacturer of 430 cm^3 using water (TEROS 10 Manual, 2022). The substantial increase of the sensing volume by 239% in wet sand compared to dry sand was mostly attributed to the additional sensing distance when the sensor was positioned with its rods vertically and with the cable facing downwards (Figure 2-5). A more detailed inspection of the responses from

each sensor configuration allowed us to quantify the response from each individual rod. Based on a side view of the TEROS 10 with the rods pointing downwards, the average sensor response extended 1.85 cm from rod one, 3.95 cm from rod two, and 1.5 cm from the tip of the rods (Figure 2-7). Based on a front view of the TEROS 10 sensor, the signal extended 1.0 cm in each direction (Figure 2-7). We did not observe any measurable signal response beyond the sensor head.

The calculations of the signal distance for TEROS 12 from the sensor reference levels resulted in measurements of 3.1 cm for the semi-major radial axis, 4.1 cm for the semi-minor radial axis, and 9.9 cm for the length of the sensor response. The resulting sensing volume of TEROS 12 in dry sand was 395 cm^3. In the case of moist sand, the semi-major radial axis measured 5.4 cm, the semi-minor radial axis measured 2.7 cm, and the length of the sensor response was 8.6 cm, resulting in a sensing volume of 394 cm^3. These values were approximately three times smaller than the manufacturer's reported value of 1,010 cm^3 using water instead of sand (TEROS 12 Manual, 2023). Based on the side view of the TEROS 12 with the rods pointing downwards, on average between dry and moist sand the sensor response 1.5 cm from rod one, 1.95 cm from rod 3, and 1.7 cm from the tip of the rods (Figure 2-7). Based on a front view of the sensor, the signal extended 2.15 cm in each direction (Figure 2-7). Similar to our findings for the TEROS 10, we did not observe any measurable signal response beyond the sensor head for the TEROS 12 sensor.

It was evident from our laboratory experiments that soil moisture largely influenced the sensing volume of TEROS 10 sensor. One possible reason for this phenomenon is that when pore spaces are filled with water, electromagnetic waves can propagate farther into the soil volume, as opposed to when the sand is dry, and the electric field has to propagate mostly through the soil

solids and air. Similar to our study, Patrignani et al. (2022) found that the soil sensing volume of soil water reflectometers was lower in dry sand with a value of 477 cm^3 when compared to the volume in deionized water, which had a value of 529 cm^3.

Discrepancies between the observed and manufacturer-reported sensing volumes may be attributed to the methodology used and the experimental error associated with laboratory methodologies. This study determined the sensing volume in both dry and wet sand, whereas previous studies used deionized water (Caldwell et al., 2018; Patrignani et al., 2022). Another factor that could explain discrepancies in the sensing volumes is the choice of the stopping criterion for determining the sensor response between our study and the sensor manufacturer. In our study we considered 95% of the maximum signal value (i.e., raw voltage value) as a reasonable threshold, but previous studies have shown that the choice of stopping criterion can substantially influence the estimated sensing volume (Patrignani et al., 2021). One question arising from this study is why the difference in sensing volume between wet and dry sand is greater for the TEROS 10 in comparison to the TEROS 12, even though both sensors are capacitance sensors using a frequency of 70 Mhz.

Conclusions

- For the TEROS 10 sensor, the third-order polynomial calibration equation with factory default parameters provided accurate soil moisture observations across three distinct soil types with an RMSE of 0.027 cm^3 cm^{-3}. The same model with fitted parameters improved the estimations of volumetric water content by 37% with an RMSE of 0.017 cm^3 cm^{-3}.
- For the TEROS 12 sensor, a linear model using either factory default parameters or fitted parameters resulted in RMSE >0.03 cm^3 cm^{-3}. A cubic polynomial model, improved the

accuracy by 32%, reducing the RMSE to 0.025 cm^3 cm^{-3}. We recommend using a cubic model to calibrate the TEROS 12 sensor instead of the default linear model.

- The sensing volume that accounted for 95% of the response of the TEROS 10 was 131 cm^3 in dry sand and 444 cm^3 in wet sand, values that are consistent with the manufacturer's specifications in water. In contrast, the sensing volume that accounted for 95% of the response of the TEROS 12 sensor exhibited a sensing volume of 395 cm^3 in dry sand and 394 cm^3 in wet sand, values that on average are about three times smaller than the reported volume of 1,010 cm^3 using water.

References

Aubert, D., Loumagne, C., & Oudin, L. (2003). Sequential assimilation of soil moisture and streamflow data in a conceptual rainfall–runoff model. *Journal of Hydrology*, *280*(1-4), 145-161. https://doi.org/10.1016/S0022-1694(03)00229-4

Baker, J. M., & Spaans, G. J. (1994). Measuring water exchange between soil and atmosphere with TDR-microdosimetry. *Soil science*, *158*(1), 22-30. https://doi.org/10.1097/00010694-199407000-00003

Brocca, L., Morbidelli, R., Melone, F., & Moramarco, T. (2007). Soil moisture spatial variability in experimental areas of central Italy. *Journal of Hydrology*, *333*(2-4), 356-373. https://doi.org/10.1016/j.jhydrol.2006.09.004

Bojinski, S., Verstraete, M., Peterson, T. C., Richter, C., Simmons, A., & Zemp, M. (2014). The concept of essential climate variables in support of climate research, applications, and policy. *Bulletin of the American Meteorological Society*, 95(9), 1431-1443. https://doi.org/10.1175/BAMS-D-13-00047.1

Bushong, J. T., Mullock, J. L., Miller, E. C., Raun, W. R., Klatt, A. R., & Arnall, D. B. (2016). Development of an in-season estimate of yield potential utilizing optical crop sensors and soil moisture data for winter wheat. *Precision Agriculture*, 17, 451-469. https://doi.org/10.1007/s11119-016-9430-4

Bwambale, E., Abagale, F. K., & Anornu, G. K. (2023). Data-driven modelling of soil moisture dynamics for smart irrigation scheduling. *Smart Agricultural Technology*, *5*, 100251. https://doi.org/10.1016/j.atech.2023.100251

Caldwell, T. G., Bongiovanni, T., Cosh, M. H., Halley, C., & Young, M. H. (2018). Field and laboratory evaluation of the CS655 soil water content sensor. *Vadose Zone Journal*, *17*(1), 1-16. https://doi.org/10.2136/vzj2017.12.0214

Cavanaugh, M. L., Kurc, S. A., & Scott, R. L. (2011). Evapotranspiration partitioning in semiarid shrubland ecosystems: A two-site evaluation of soil moisture control on transpiration. *Ecohydrology*, *4*(5), 671-681. https://doi.org/10.1002/eco.157

Cosh, M. H., Ochsner, T. E., McKee, L., Dong, J., Basara, J. B., Evett, S. R., ... & Sayde, C. (2016). The soil moisture active passive Marena, Oklahoma, in situ sensor testbed (SMAP-MOISST): Testbed design and evaluation of in situ sensors. *Vadose Zone Journal*, 15(4), vzj2015-09. https://doi.org/10.2136/vzj2015.09.0122

Ding, R., Kang, S., Zhang, Y., Hao, X., Tong, L., & Du, T. (2013). Partitioning evapotranspiration into soil evaporation and transpiration using a modified dual crop coefficient model in irrigated maize field with ground-mulching. *Agricultural Water Management*, *127*, 85-96. https://doi.org/10.1016/j.agwat.2013.05.018

Elder, A. N., & Rasmussen, T. C. (1994). Neutron probe calibration in unsaturated tuff. *Soil Science Society of America Journal*, *58*(5), 1301-1307, https://doi.org/10.1071/SR03051

Eltahir, E. A. B. (1998). A soil moisture–rainfall feedback mechanism: 1. Theory and observations. *Water Resources Research*, *34*(4), 765-776. https://doi.org/10.1029/97WR03499

Evett, S. R., Tolk, J. A., & Howell, T. A. (2005). Time domain reflectometry laboratory calibration in travel time, bulk electrical conductivity, and effective frequency. *Vadose Zone Journal*, *4*(4), 1020-1029. https://doi.org/10.2136/vzj2005.0046

Evett, S. R., Tolk, J. A., & Howell, T. A. (2006). Soil profile water content determination: sensor accuracy, axial response, calibration, temperature dependence, and precision. *Vadose Zone Journal*, *5*(3), 894-907. https://doi.org/10.2136/vzj2005.0149

Fares, A., & Alva, A. K. (2000). Evaluation of capacitance probes for optimal irrigation of citrus through soil moisture monitoring in an entisol profile. *Irrigation Science*, 19, 57-64. https://doi.org/10.1007/s002710050001

Flynn, K. D., Wyatt, B. M., & McInnes, K. J. (2021). Novel cosmic ray neutron sensor accurately captures field-scale soil moisture trends under heterogeneous soil textures. *Water*, *13*(21), 3038. https://doi.org/10.3390/w13213038

Gavlak, R., Horneck, R., & Miller, R. O. (2005). Particle size analysis: Hydrometer method.

Geesing, D., Bachmaier, M., & Schmidhalter, U. (2004). Field calibration of a capacitance soil water probe in heterogeneous fields. *Soil Research*, *42*(3), 289-299. https://doi.org/10.1071/SR03051

Gu, L., Meyers, T., Pallardy, S. G., Hanson, P. J., Yang, B., Heuer, M., Hosman, K. P., Riggs, J. S., Sluss, D., & Wullschleger, S. D. (2006). Direct and indirect effects of atmospheric conditions and soil moisture on surface energy partitioning revealed by a prolonged drought at a temperate forest site. *Journal of Geophysical Research: Atmospheres*, 111(D16). https://doi.org/10.1029/2006JD007161

Hanson, B., Orloff, S., & Peters, D. (2000). Monitoring soil moisture helps refine irrigation management. *California Agriculture*, 54(3), 38-42. https://doi.org/10.3733/ca.v054n03p38

Hollmann, R., Merchant, C. J., Saunders, R., Downy, C., Buchwitz, M., Cazenave, A., ... & Wagner, W. (2013). The ESA climate change initiative: Satellite data records for

essential climate variables, B. *American Meteorological Society*., 94, 1541–1552. https://doi.org/10.1175/BAMS-D-11-00254.1

Holzman, M., Rivas, R., & Piccolo, M. (2014). Estimating soil moisture and the relationship with crop yield using surface temperature and vegetation index. *International Journal of Applied Earth Observation and Geoinformation*, *28*, 181-192. https://doi.org/10.1016/j.jag.2013.12.006

Irmak, S., Haman, D. Z., & Bastug, R. (2000). Determination of crop water stress index for irrigation timing and yield estimation of corn. *Agronomy Journal*, *92*(6), 1221-1227. https://doi.org/10.2134/agronj2000.9261221x

Jones, S. B., Wraith, J. M., & Or, D. (2002). Time domain reflectometry measurement principles and applications. *Hydrological Processes*, *16*(1), 141-153. https://doi.org/10.1002/hyp.513

Kargas, G., & Soulis, K. X. (2019). Performance evaluation of a recently developed soil water content, dielectric permittivity, and bulk electrical conductivity electromagnetic sensor. *Agricultural Water Management*, 213, 568-579. https://doi.org/10.1016/j.agwat.2018.11.002

Kirkby, M. (1988). Hillslope runoff processes and models. *Journal of Hydrology*, *100*(1-3), 315-339. https://doi.org/10.1016/0022-1694(88)90190-4

Kumar, M., Kumar, A., & Palaparthy, V. S. (2020). Soil sensors-based prediction system for plant diseases using exploratory data analysis and machine learning. *IEEE Sensors Journal*, 21(16), 17455-17468. https://doi.org/10.1109/JSEN.2020.3046295

Ledieu, J., De Ridder, P., De Clerck, P., & Dautrebande, S. (1986). A method of measuring soil moisture by time-domain reflectometry. *Journal of Hydrology*, 88(3-4), 319-328. https://doi.org/10.1016/0022-1694(86)90097-1

Martínez-Gimeno, M., Jiménez-Bello, M., Lidón, A., Manzano, J., Badal, E., Pérez-Pérez, J., Bonet, L., Intrigliolo, D., & Esteban, A. (2020). Mandarin irrigation scheduling by means of frequency domain reflectometry soil moisture monitoring. *Agricultural Water Management, 235*, 106151. https://doi.org/10.1016/j.agwat.2020.106151

METER Group, Inc. (2022). *TEROS 11/12: 18225-07* (11.2022). METER Group, Inc.

METER Group, Inc. (2023). *TEROS 10: 18241-06* (5.2023). METER Group, Inc.

METER Group, Inc (2022). Measurement Volume: The meter volumetric water content sensors. [Online]. https://publications.metergroup.com/Sales%20and%20Support/METER%20Environment/Website%20Articles/measurement-volume-meter-volumetric-water-content-sensors.pdf

Mohamed, A. Z., Osroosh, Y., Peters, R. T., Bates, T., Campbell, C. S., & Ferrer-Alegre, F. (2021). Monitoring water status in apple trees using a sensitive morning crop water stress index*. *Irrigation and Drainage, 70*(1), 27-41. https://doi.org/10.1002/ird.2528

Ojo, E. R., Bullock, P. R., L'Heureux, J., Powers, J., McNairn, H., & Pacheco, A. (2015). Calibration and evaluation of a frequency domain reflectometry sensor for real-time soil moisture monitoring. *Vadose Zone Journal*, 14(3), vzj2014-08. https://doi.org/10.2136/vzj2014.08.0114

Or, D., & Wraith, J. M. (1999). Temperature effects on soil bulk dielectric permittivity measured by time domain reflectometry: A physical model. *Water Resources Research*, *35*(2), 371-383. https://doi.org/10.1029/1998WR900008

Ortega-Farías, S. O., & Acevedo, C. (2004). Irrigation scheduling on vineyards (Viith Region of Chile) by using the time domain reflectometry. In *Bridging the Gap: Meeting the World's Water and Environmental Resources Challenges* (pp. 1-6). https://doi.org/10.1061/40569(2001)343

Patle, K. S., Saini, R., Kumar, A., & Palaparthy, V. S. (2021). Field evaluation of smart sensor system for plant disease prediction using LSTM network. *IEEE Sensors Journal*, 22(4), 3715-3725. https://doi.org/10.1109/JSEN.2021.3139988

Patrignani, A., Ochsner, T. E., Feng, L., Dyer, D., & Rossini, P. R. (2022). Calibration and validation of soil water reflectometers. *Vadose Zone Journal*, *21*(3), e20190. https://doi.org/10.1002/vzj2.20190

Patrignani, A., Parker, N., & Cominelli, S. (2022). Upland rootzone soil water deficit regulates streamflow in a catchment dominated by North American Tallgrass Prairie. *Water, 14*(5), 759. https://doi.org/10.3390/w14050759

Polyakov, V., Fares, A., & Ryder, M. H. (2005). Calibration of a capacitance system for measuring water content of tropical soil. *Vadose Zone Journal*, *4*(4), 1004-1010. https://doi.org/10.2136/vzj2005.0028

Rigden, A. J., Salvucci, G. D., Entekhabi, D., & Short Gianotti, D. J. (2018). Partitioning evapotranspiration over the continental United States using weather station data. *Geophysical Research Letters*, *45*(18), 9605-9613. https://doi.org/10.1029/2018GL079121

Rockström, J., Jansson, P., & Barron, J. (1998). Seasonal rainfall partitioning under runon and runoff conditions on sandy soil in Niger. On-farm measurements and water balance

modelling. *Journal of Hydrology*, *210*(1-4), 68-92. https://doi.org/10.1016/S0022-1694(98)00176-0

Rossini, P. R., Ciampitti, I. A., Hefley, T., & Patrignani, A. (2021). A soil moisture-based framework for guiding the number and location of soil moisture sensors in agricultural fields. *Vadose Zone Journal*, *20*(6), e20159. https://doi.org/10.1002/vzj2.20159

Scanlon, T. M., & Kustas, W. P. (2012). Partitioning evapotranspiration using an eddy covariance-based technique: Improved assessment of soil moisture and land–atmosphere exchange dynamics. *Vadose Zone Journal*, 11(3), vzj2012-0025. https://doi.org/10.2136/vzj2012.0025

Schaap, M., De Lange, L., & Heimovaara, T. (1997). TDR calibration of organic forest floor media. *Soil Technology*, *11*(2), 205-217. https://doi.org/10.1016/S0933-3630(96)00128-6

Scott, R. L., Knowles, J. F., Nelson, J. A., Gentine, P., Li, X., Barron-Gafford, G., Bryant, R., & Biederman, J. A. (2021). Water availability impacts on evapotranspiration partitioning. *Agricultural and Forest Meteorology*, *297*, 108251. https://doi.org/10.1016/j.agrformet.2020.108251

Topp, G. C., Davis, J. L., & Annan, A. P. (1980). Electromagnetic determination of soil water content: Measurements in coaxial transmission lines. *Water Resources Research*, *16*(3), 574-582. https://doi.org/10.1029/WR016i003p00574

Topp, G. C., & Reynolds, W. D. (1998). Time domain reflectometry: A seminal technique for measuring mass and energy in soil. *Soil and Tillage Research*, 47(1-2), 125-132. https://doi.org/10.1016/S0167-1987(98)00083-X

Tramblay, Y., Bouvier, C., Martin, C., Didon-Lescot, J., Todorovik, D., & Domergue, J. (2010). Assessment of initial soil moisture conditions for event-based rainfall–runoff modelling. *Journal of Hydrology, 387*(3-4), 176-187. https://doi.org/10.1016/j.jhydrol.2010.04.006

Vaz, C. M., Jones, S., Meding, M., & Tuller, M. (2013). Evaluation of standard calibration functions for eight electromagnetic soil moisture sensors. *Vadose Zone Journal*, 12(2), vzj2012-0160. https://doi.org/10.2136/vzj2012.0160

Walker, J. P., Willgoose, G. R., & Kalma, J. D. (2001). The Nerrigundah data set: Soil moisture patterns, soil characteristics, and hydrological flux measurements. *Water Resources Research*, *37*(11), 2653-2658. https://doi.org/10.1029/2001WR000545

Walsh, O. S., Klatt, A. R., Solie, J. B., Godsey, C. B., & Raun, W. R. (2013). Use of soil moisture data for refined GreenSeeker sensor based nitrogen recommendations in winter wheat (Triticum aestivum L.). *Precision Agriculture,* 14, 343-356. https://doi.org/10.1007/s11119-012-9299-9

Western, A. W., & Grayson, R. B. (1998). The Tarrawarra data set: Soil moisture patterns, soil characteristics, and hydrological flux measurements. *Water Resources Research*, *34*(10), 2765-2768. https://doi.org/10.1029/98WR01833

Wraith, J. M., & Or, D. (1999). Temperature effects on soil bulk dielectric permittivity measured by time domain reflectometry: Experimental evidence and hypothesis development. *Water Resources Research*, *35*(2), 361-369. https://doi.org/10.1029/1998WR900006

Zhao, P., Kang, S., Li, S., Ding, R., Tong, L., & Du, T. (2018). Seasonal variations in vineyard ET partitioning and dual crop coefficients correlate with canopy development and surface soil moisture. *Agricultural Water Management*, *197*, 19-33. https://doi.org/10.1016/j.agwat.2017.11.004

Zotarelli, L., Dukes, M., Scholberg, J., Muñoz-Carpena, R., & Icerman, J. (2009). Tomato nitrogen accumulation and fertilizer use efficiency on a sandy soil, as affected by nitrogen rate and irrigation scheduling. *Agricultural Water Management*, *96*(8), 1247-1258. https://doi.org/10.1016/j.agwat.2009.03.019

Zotarelli, L., Dukes, M. D., Scholberg, J. M. S., Femminella, K., & Munoz-Carpena, R. (2011). Irrigation scheduling for green bell peppers using capacitance soil moisture sensors. *Journal of irrigation and drainage engineering*, 137(2), 73-81. https://doi.org/10.1061/(ASCE)IR.1943-4774.0000281

Table 2-1 Soil textural class, percentage of sand, percentage of clay, actual bulk density (ρ_b) from soil sample, bulk electrical conductivity (EC_b), range in volumetric water content (VWC) of the packed soil columns, and organic matter (OM) of the three soils used in the calibration of the TEROS 10 and TEROS 12 soil moisture sensors.

Soil textural class	**Sand**†	**Clay**†	**ρ_b**	**EC_b**	**VWC range**	**OM**‡
	%	%	g cm^{-3}	dS m^{-1}	cm^3 cm^{-3}	%
Sand	100	0	1.7	0 – 0.181	0.001 – 0.320	0
Loam	42	13	1.3	0 – 0.263	0.005 – 0.449	1.5
Silty clay loam	10	28	1.1	0 – 0.347	0.009 – 0.463	3.1

†Particle size was determined using the hydrometer method (Gavlak et al., 2005)
‡Organic matter was determined using the loss on ignition method. Samples were analyzed by the Kansas State University Soil Testing Lab.

Table 2-2 Parameter values (*a*, *b*, *c*, *d*), coefficient of determination (R^2), root mean square error (RMSE), and mean absolute error (MAE) for the factory and fitted calibration equations for the TEROS 10 and TEROS 12 sensors.

Sensor	**Equation**	***a***	***b***	***c***	***d***	R^2	**RMSE** $cm^3\ cm^{-3}$	**MAE** $cm^3\ cm^{-3}$
TEROS 10	Cubic Factory	4.824×10^{-10}	-2.278×10^{-6}	3.899×10^{-3}	2.51	0.97	0.027	0.020
TEROS 10	Cubic Fitted	8.916×10^{-10}	-4.136×10^{-6}	6.673×10^{-3}	3.50	0.99	0.017	0.015
TEROS 12	Linear Factory	3.879×10^{-4}	-0.70			0.94	0.037	0.033
TEROS 12	Linear Fitted	4.223×10^{-4}	-0.77			0.94	0.035	0.030
TEROS 12	Cubic Fitted	1.211×10^{-9}	-8.643×10^{-6}	2.078×10^{-2}	-16.5	0.97	0.025	0.020

Table 2-3 Response of TEROS 10 and TEROS 12 in oven-dry and moist (0.100 cm^3 cm^{-3}) sand.

	TEROS 10			TEROS 12		
Sensor orientation	**Dry**	**Wet**	**Mean**	**Dry**	**Wet**	**Mean**
	cm	cm	cm	cm	cm	cm
Rods vertical with cable upwards	5.2	5.2	5.2	3.2	5.8	4.5
Rods vertical with cable	1.5	4.7	3.1	3.0	5.0	4
Rods horizontal	1.5	3.1	2.3	4.1	2.7	3.4
Rods facing upwards	6.5	7.3	6.9	7.6	6.8	7.2
Rods facing downwards	1.8	1.9	1.9	2.3	1.8	2.1

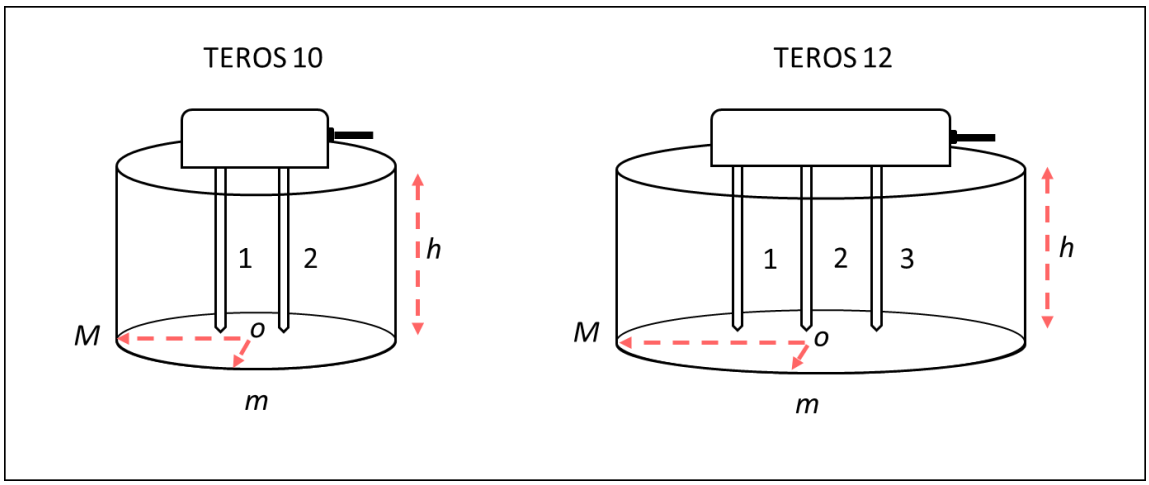

Figure 2-1 Sketch illustrating the semi-major radial axis (*M*), the semi-minor radial axis (*m*), and the sensing height (*h*), where *o* is the center from which semi-major and semi-minor radial axes were measured for the elliptical cylinder formula adopted to estimate the sensing volume for the TEROS soil moisture sensors. The individual sensor rods are denoted with the numbers 1, 2, and 3.

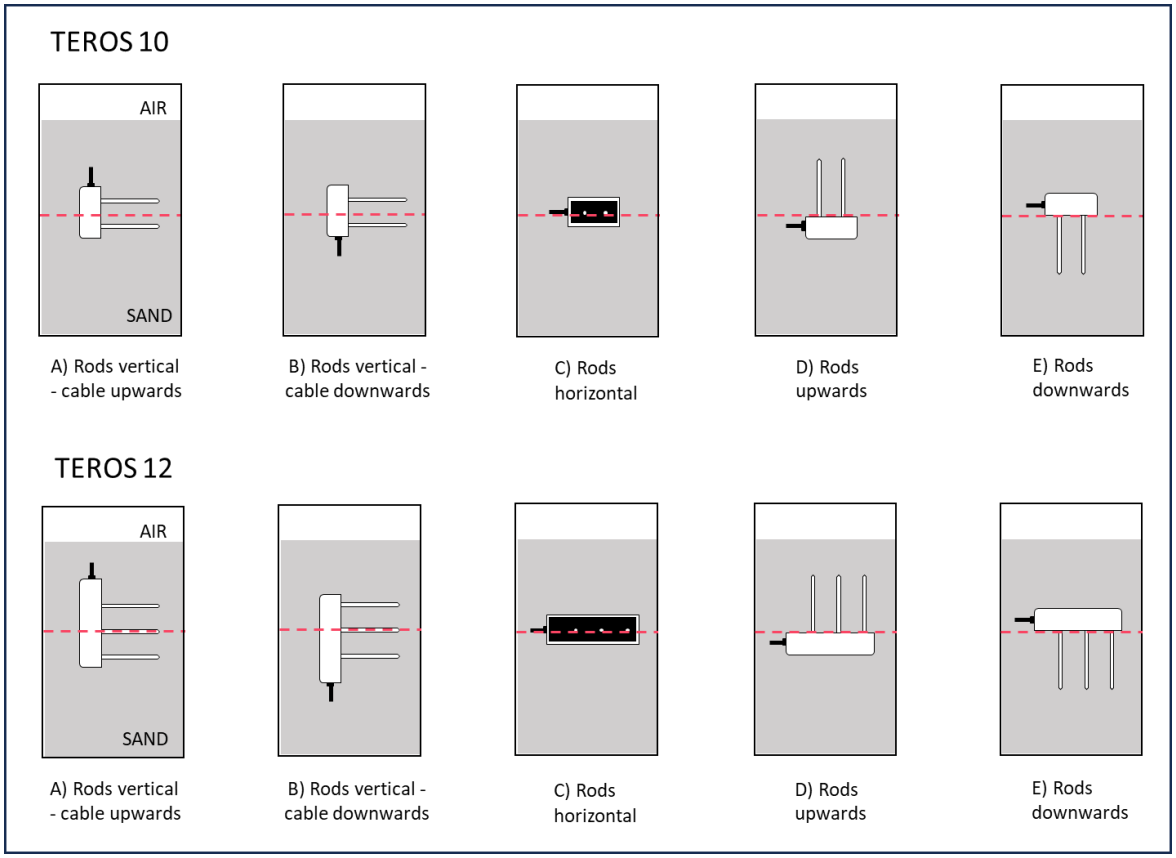

Figure 2-2 Sketch (not to scale) illustrating the orientations of the TEROS 10 and TEROS 12 soil moisture sensors during the determination of the sensing volume. The experiments were conducted in 20,612 cm^3 cylindrical containers that were gradually filled with increasing levels of oven-dry and moist (0.100 cm^3 cm^{-3}) fine sand (<1 mm diameter). The red dashed line represents the reference level used as the center of the elliptical cylinder. The sensors with the rods oriented vertically were used to compute the semi-major radial axis, the sensor with rods in horizontal position were used to compute the semi-minor radial axis, and the sensor with the rods pointing upwards and downwards was used to compute the height.

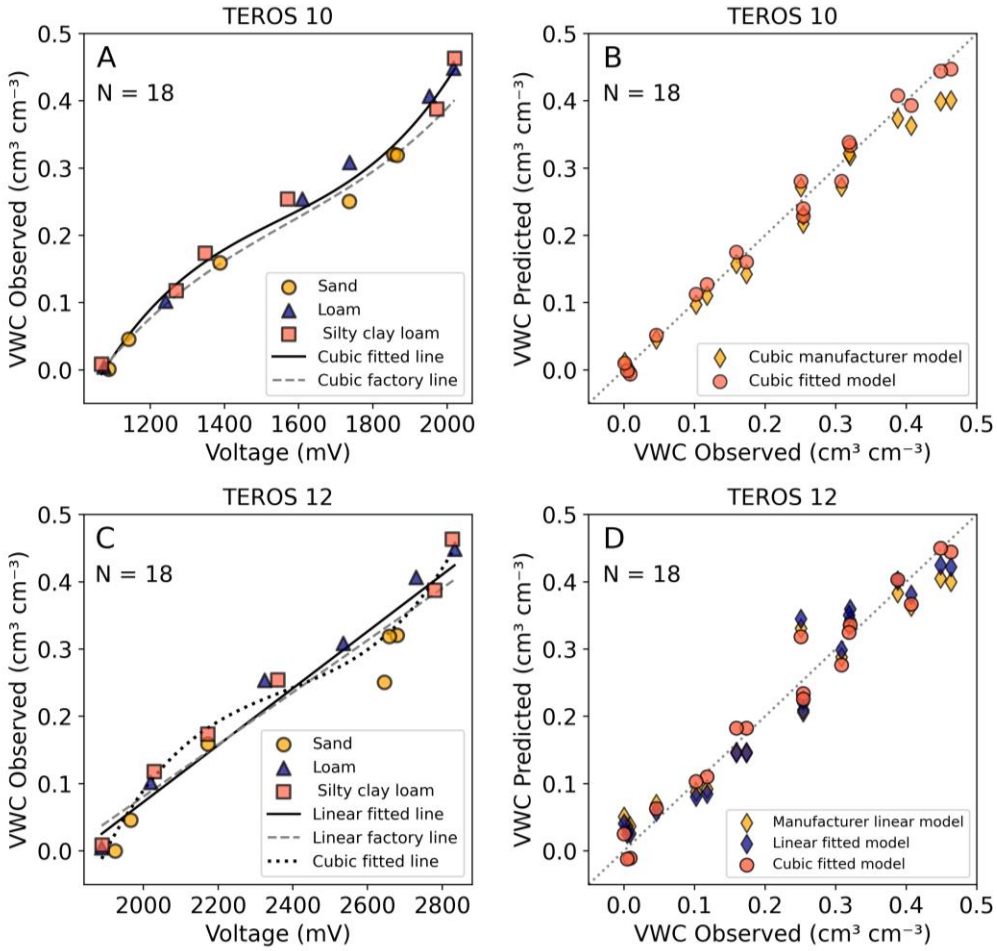

Figure 2-3 Relationship between raw voltage output (*Voltage*, mV) and observed volumetric water content (VWC Observed) determined by the thermo-gravimetric method for the three tested soils (A and C). One-to-one relationship between the VWC Observed and VWC determined using the manufacturer's and fitted calibration equations (B and D).

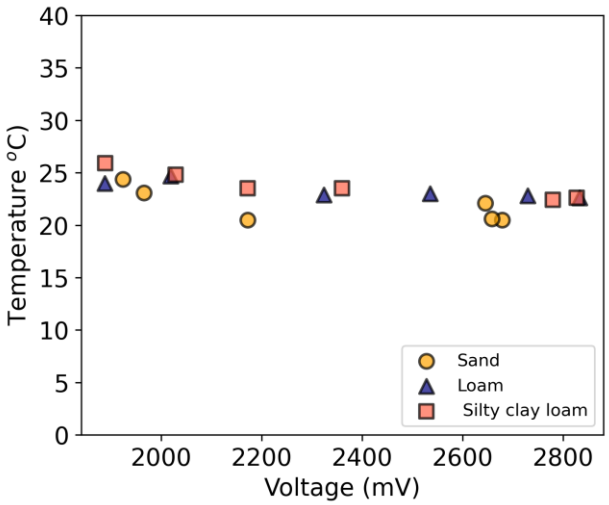

Figure 2-4 Range of temperature during the laboratory calibration based on TEROS 12 measurements.

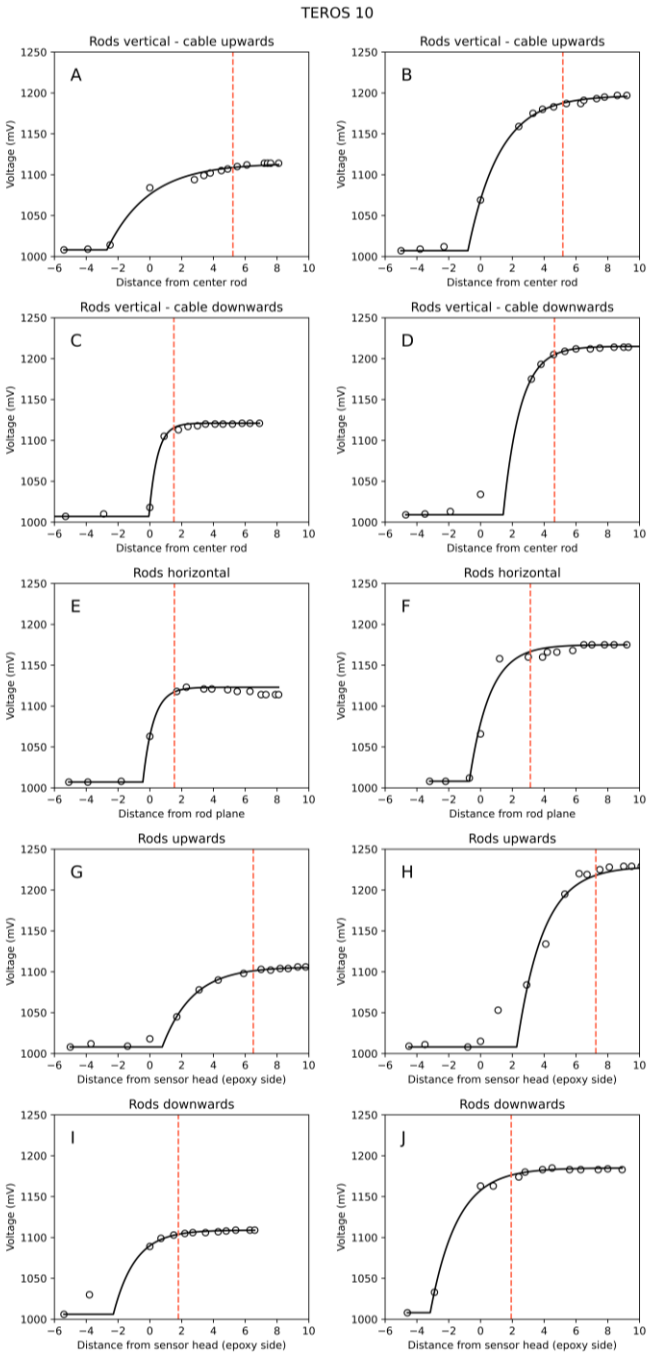

Figure 2-5 Response of the TEROS 10 in terms of raw voltage output as a function of the distance from the reference point (for additional reference see dashed lines in Figure 2-2) for the oven-dry (left column, A, C, E, G, and I) and moist (0.100 cm^3 cm^{-3}) sand (right column, B, D, F, H, and J). Vertical dashed lines represent 95% of the sensor's maximum response. Panels A, B, C, and D represent the magnitude of the semi-major radial axis. Panels E and F represent the magnitude of the semi-minor radial axis. Panels G, H, I, and J represent the height of the elliptical cylinder.

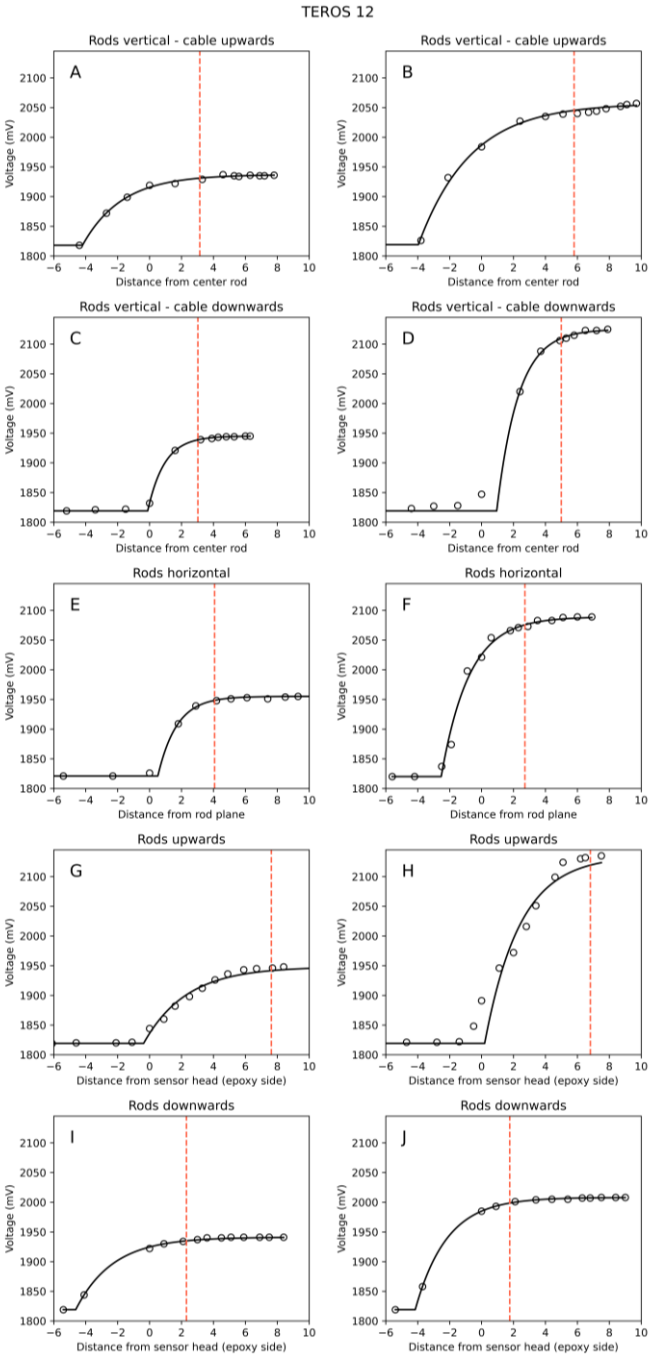

Figure 2-6 Response of the TEROS 12 in terms of raw voltage output as a function of the distance from the reference point (for additional reference see dashed lines in Figure 2-2) for the oven-dry (left column, A, C, E, G, and I) and moist sand (0.100 cm^3 cm^{-3}) (right column, B, D, F, H, and J). Vertical dashed lines represent 95% of the sensor's maximum response. Panels A, B, C, and D represent the magnitude of the semi-major radial axis. Panels E and F represent the magnitude of the semi-minor radial axis. Panels G, H, I, and J represent the height of the elliptical cylinder.

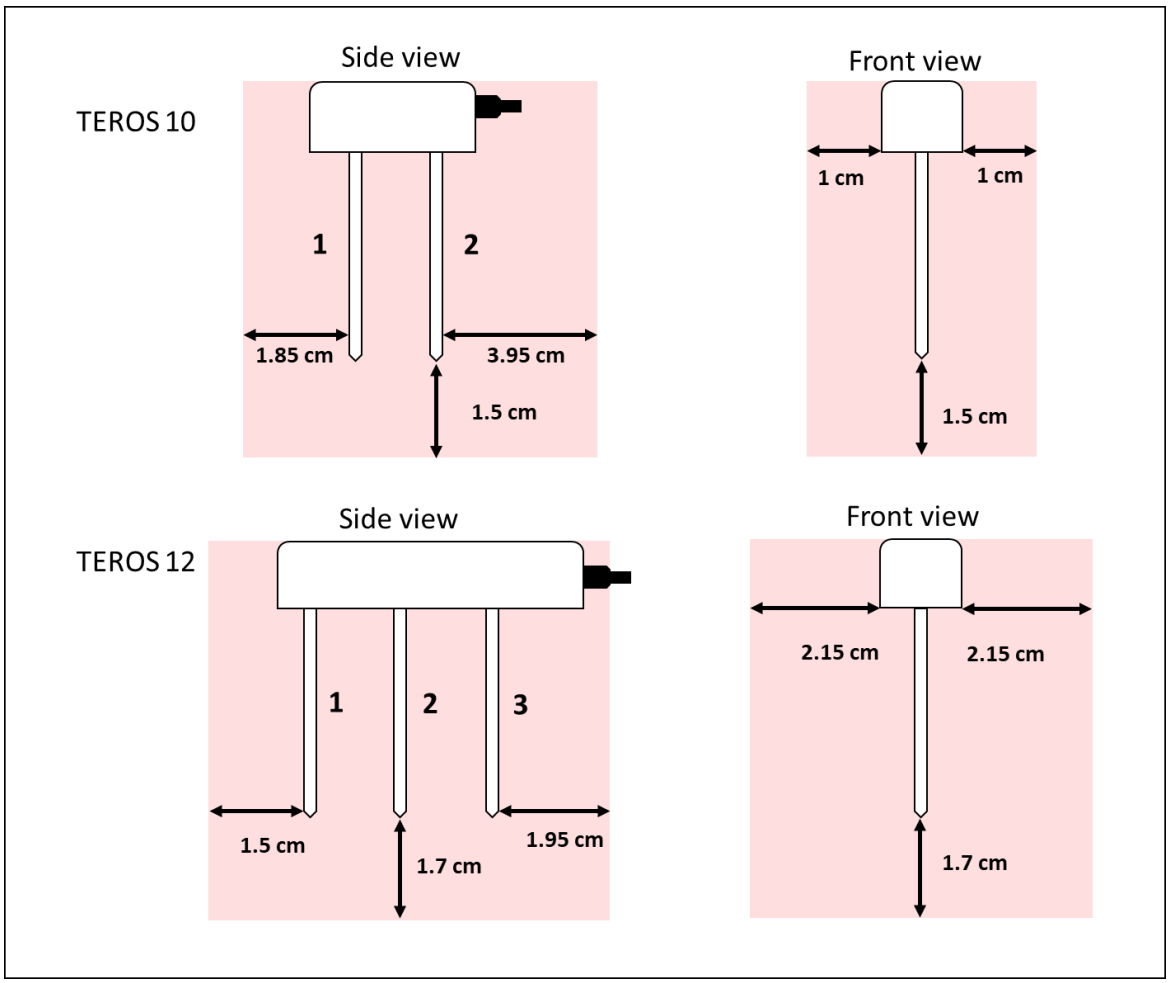

Figure 2-7 Sketch (not to scale) illustrating the magnitude of the average signal responses in dry and wet sand for the TEROS 10 and TEROS 12 sensors.

Chapter 3 - Quantifying *In Situ* Soil Evaporation Using a Model-Data Assimilation Approach

Abstract

Soil evaporation is a major component of the soil water balance in rainfed cropping systems of the U.S. Great Plains, accounting for ~40% of the annual precipitation losses. A common method to quantify soil evaporation rate consists of using microlysimeters, which are thin-walled cylinders inserted into the soil, sealed at the bottom, and weighed daily to estimate evaporation loss for short periods of time. However, the use of microlysimeters is labor-intensive and relies on manual measurements. The objective of the study was to develop and test a model-data assimilation approach that combines a simple evaporation model with a) surface soil moisture measured with a sensor and b) canopy cover estimated from downward-facing images to quantify soil evaporation rate during two winter wheat growing seasons and bare soil. Soil evaporation rate was simulated with the FAO-56 Dual Crop Coefficient (DualKc) model. The soil moisture and the canopy cover observations were assimilated into the model using the direct insertion method, resulting in a total of five approaches to test. All the approaches were validated with the traditional microlysimeter technique. Results indicated that assimilating canopy cover into the DualKc model proved to be a promising approach for estimating soil evaporation in winter wheat, yielding an average RMSE of 0.6 mm day^{-1} over two growing seasons. A well-parameterized DualKc model also demonstrated accuracy in estimating soil evaporation in winter wheat, with an RMSE of 0.6 mm day^{-1}, while assimilating soil moisture resulted in a higher RMSE of 1.2 mm day^{-1}. In bare soil conditions, the most effective approach for estimating soil evaporation involved assessing changes in soil water storage based on differences in soil moisture in the top 12 cm of the soil profile, resulting in an RMSE of 0.6 mm day^{-1}. These

findings show that improving the partition of energy through the assimilation of canopy cover may be better than improving the surface soil moisture status based on soil moisture sensors for determining soil evaporation rates using data-driven approaches.

Introduction

At the global scale, the evapotranspiration (ET) process represents about 65% of the annual terrestrial precipitation (Oki & Kanae, 2006; Trenberth et al., 2007; Rodell et al., 2011), with evaporation from the soil, litter, and canopy surfaces accounting for approximately 20-40% of the total ET (Merlin et al., 2016). In the U.S. Great Plains, approximately 75% of the cultivated land relies on natural precipitation for crop production (Baumhardt & Salinas-Garcia, 2006), where soil evaporation can reach magnitudes equal to or even exceed that of plant transpiration, especially in the case of field crops with periods having incomplete soil cover or fallow periods with bare soil conditions. For instance, a global ET partitioning modeling study, which was part of the Coupled Model Intercomparison Project (CMIP), estimated that soil evaporation can account for 30-40% of total ET in the U.S. Great Plains (Berg & Sheffield, 2019). Similarly, a global study using the Community Land Model (CLM) and remote sensing information estimated that soil evaporation typically ranges from 40-50% of the total ET in this region (Lawrence et al., 2007). A study investigating the magnitude of yield gaps and possible causes of yield stagnation in winter wheat (*Triticum aestivum* L.) in Oklahoma revealed that about 70% of the annual precipitation is lost due to soil evaporation (Patrignani et al., 2014) and another study in Oklahoma using a simplified soil water balance estimated that ~59% of the annual precipitation received by rainfed cropland under continuous winter wheat is lost in the form of unproductive evaporative losses (Warren et al., 2009). Given the large impact of unproductive evaporative losses in this region, accurate measurements of soil evaporation rates play a crucial role in scientific research focused on studying the components of the soil water balance and evaluating more effective soil water conservation practices.

Perhaps, the most common, direct, and reliable method for measuring *in situ* soil evaporation during both the energy-limiting and the water-limiting stages is the microlysimeter technique (Boast & Robertson, 1982; Evett et al., 1995). Microlysimeters are cylinders inserted into the soil, excavated, sealed at the bottom, and weighed daily to estimate soil evaporation loss for short periods of time. The microlysimeter technique has been widely used to directly quantify *in situ* soil evaporation across a wide range of ecosystems and regions of the world, including bare soil conditions (Boast and Robertson, 1982; Daamen et al., 1993; Flumignan et al., 2012), irrigated crops like corn (*Zea mays* L.), cotton (*Gossypium hirsutum* L.), and sunflower (*Helianthus annuus* L.) (Klocke et al., 1996; Jara et al., 1998; Villalobos and Fereres, 1990), furrow- and drip-irrigated vineyards (Kool et al., 2016; Zhao et al., 2018), a mesic tallgrass prairie (da Rocha et al., 2022), African savanna ecosystems (Metzger et al., 2014), and the arid Patagonia steppe (Paruelo et al., 1991). However, major drawbacks of the microlysimeter technique are the small measurement area, the amount of labor required to install and periodically weigh the microlysimeters, and the fact that the soil moisture within the microlysimeter volume starts to diverge from that of the surrounding soil within a few days as roots uptake water from the surrounding soil and capillary flow at the bottom of the microlysimeter is restricted. Thus, for accurate measurements of soil evaporation rate, researchers often need to install new microlysimeters, which makes this technique very labor-intensive and only practical for sporadic measurements over short periods of time along the growing season. To extend the lifetime of field microlysimeters, improve the temporal resolution of soil evaporation measurements, and avoid daily weighing, researchers have explored coupling microlysimeters with soil moisture sensors to continuously estimate soil evaporation rate based on changes in soil water storage. For instance, in a study using a 20-cm long microlysimeter that

was equipped with a time domain reflectometry (TDR) waveguide and sealed at the bottom with a few perforations for drainage, researchers obtained soil evaporation estimates that closely matched observations with a Bowen ratio system (Baker and Spaans, 1994). The method suggested by Baker & Spaans (1994) was the first attempt at instrumenting microlysimeters with soil moisture sensors. One advantage of this method is the addition of drainage holes to allow excess moisture to leave the microlysimeter after large rainfall events or snowmelt. Two practical limitations of this initial concept are 1) waveguides were inserted from the bottom, which require excavation, and 2) excavation and sealing of the bottom of the microlysimeter disrupts pore connectivity, which my limit accuracy during extended drydown periods.

Alternative methods to the microlysimeter technique for measuring soil evaporation rate include heat pulse sensors and eddy covariance. Heat pulse probes are small sensors that can collect accurate measurements near the soil surface to compute the surface energy balance for a specific soil layer between two measurement depths (Campbell et al., 1991, Bristow et al., 1994). This technique is best suited for studying soil evaporation rate during drydown periods as it cannot measure evaporation rate during the energy-limited stage (Deol et al., 2012). The eddy covariance method has been widely used to measure high frequency (i.e., 10 Hz or higher) observations of the exchange of carbon dioxide and water vapor fluxes simultaneously at the landscape level. The methodology can provide direct and continuous measurements of ET (Wagle et al., 2020), but ET partitioning requires separate measurements for soil evaporation and plant transpiration (Wagle et al., 2020) or data processing methods like the underlying water use efficiency approach developed by Zhou et al. (2016).

Because quantifying *in situ* soil evaporation requires either a labor-intensive set up or expensive instrumentation (e.g., eddy covariance system), physically-based and empirical

models are solutions for estimating soil evaporation rates across various temporal and spatial scales, minimizing the need for extensive fieldwork. A widely used physically-based model for estimating soil evaporation is HYDRUS 1D (Šimunek et al., 2012), which can simulate soil water and heat dynamics numerically, and can estimate soil evaporation based on potential ET and soil hydraulic properties. In an irrigated winter wheat study, HYDRUS was used for estimating actual evapotranspiration, soil evaporation, and crop transpiration, with validation against the eddy covariance method and a lysimeter resulting in root mean square errors (RMSE) of 0.54 mm day^{-1}, 0.73 mm day^{-1}, and 0.65 mm day^{-1}, respectively (Er-Raki et al., 2021). An empirical soil water balance model commonly used for estimating soil evaporation is the FAO-56 Dual Crop Coefficient model (Allen et al., 1998), which is based on a two-layer soil profile, where a surface layer mostly accounts for soil evaporation and a rootzone layer accounts for root water uptake. The soil evaporation efficiency that controls the energy-limiting and water-limiting stages of soil evaporation is described by a linear-plateau model. Previous models, like the Bucket model (Manabe, 1969; Robock et al., 1995), have used these simplified relationships to describe soil evaporation rate as a function surface soil moisture. Newer and more advanced models represent the soil evaporation efficiency using continuous non-linear relationships (Lie and Pielke 1992; Merlin et al., 2011; Oleson et al., 2013).

Models describing the soil water balance that estimate soil evaporation through a robust relationship with surface soil moisture represent an opportunity for data-driven approaches. These approaches could integrate *in situ* observations of soil moisture with weather data sourced from mesoscale environmental monitoring networks. In this study, we hypothesize that a model-data assimilation approach that combines observations of surface soil moisture and green canopy cover will be more accurate than using a soil evaporation model or *in situ* surface soil moisture

observations alone. The objective of the study was to develop and test a model-data assimilation approach that combines a simple evaporation model with surface soil moisture (SSM) observations obtained from an instrumented microlysimeter and canopy cover estimated from downward-facing images to quantify soil evaporation rate during the growing season and fallow periods.

Materials and Methods

Description of experimental site

The study was conducted at the Kansas State University Ashland Bottoms Experiment Station near Manhattan, KS during the 2021/2022 and 2022/2023 winter wheat growing seasons, and in bare soil during the summer of 2023. In 2021/2022, winter wheat (Zenda variety) was planted on 22 October 2021 at a density of 38 plants m^{-2}, a row spacing of 0.19 m, and fertilized with 90 kg ha^{-1} of N (source Urea Ammonium Nitrate, 32-0-0 of N–P2O5–K2O) as an in-furrow starter fertilizer. To control weeds, spring herbicide applications consisted of mixtures of Harmony® Extra (thifensuifuron-methyl), MCPA, and NIS® (nonionic surfactant), and herbicides mixtures were applied during fallow periods to suppress weeds when needed. Neither insecticides nor fungicides were applied to the plots. In 2022/2023, the same variety of winter wheat was planted on 15 October 2022 using the same management as in the previous season. Winter wheat plots (12.19 m wide and 15.24 m long) were replicated four times and had a rotation of continuous wheat since 2019 under no-tillage. The soil of the experimental site corresponds to the Wymore series (Fine, smectitic, mesic Aquertic Argiudolls) and had a silty clay loam (sand 10%, clay 28%) soil textural class as determined by particle size analysis using the hydrometer method (Gavlak et al., 2005). The field experiment in bare soil conditions was

conducted from 24 June to 11 August 2023 in a soil mapped as a Stonehouse series (Sandy, mixed, mesic Typic Udifluvents) and had a loam (sand 42% and clay 13%) soil textural class based on particle size analysis. During this experiment, weeds were manually controlled in a plot of 10 m by 7 m.

Soil evaporation model

Soil evaporation rate was modeled using the Dual Crop Coefficient (DualKc) method (Allen et al., 1998). The DualKc method simulates actual crop ET using a two-layer soil water balance model at daily time steps. The top soil layer is often used to represent evaporative losses, which typically dominate in the top 10 to 15 cm of the soil profile, while the bottom layer is used to represent plant water uptake in the rootzone. In this study we only considered the routines for modeling soil evaporation rate (E, mm) assuming a soil layer of 12 cm as follows:

$$E = K_e \, ET_o \quad [3.1]$$

where K_e (dimensionless) is the soil evaporation coefficient and ET_o (mm d^{-1}) is reference ET for a hypothetical non-water limited grass surface that is 0.12 m in height, with a surface resistance of 70 s m^{-1}, and an albedo of 0.23. In this study, daily grass ET_o was obtained using the formulation of the Penman-Monteith equation as detailed in the FAO-56 manual (Allen et al., 1998):

$$ET_o = \frac{0.408\,\Delta\,(R_n - G) + \frac{900}{T_a+273}\,\gamma u_2\,(e_s - e_a)}{\Delta + \gamma\,(1 + 0.34u_2)} \quad [3.2]$$

where R_n is net radiation at the crop surface (MJ m^{-2} d^{-1}), G is the soil heat flux (MJ m^{-2} d^{-1}), T_a is the daily average air temperature at a height of 2 meters (˚C), u_2 (m s^{-1}) is the daily mean wind speed at a reference height of 2 meters, e_s is the saturation vapor pressure (kPa), e_a is the actual vapor pressure (kPa), Δ is the slope of the vapor pressure curve (kPa ˚C^{-1}), and γ is the

psychrometric constant (kPa $^{\circ}C^{-1}$). The value of K_e ranges from zero when the soil surface is dry to its maximal value (K_e ~1.2) shortly after precipitation or irrigation events when the soil surface is wet and soil evaporation is mostly limited by the supply of energy:

$$K_e = K_r(K_{c\,max} - K_{cb}) \leq f_{ew}\ K_{c\,max} \qquad [3.3]$$

where K_r is the evaporation reduction coefficient, which is also known as the soil evaporation efficiency (e.g., Merlin et al., 2016), $K_{c\,max}$ is the maximum value of the crop coefficient following rain or irrigation, K_{cb} is the basal crop coefficient that varies with crop stages and that typically ranges from 0.15 to 1.10 , and f_{ew} is the fraction of the soil that is wetted and exposed to incident solar radiation. The value of f_{ew} is estimated based on the fraction of canopy cover (f_c) and the fraction of the wetted soil surface (f_w) by precipitation (i.e., $f_w = 1$):

$$f_{ew} = min\,(1 - f_c, f_w\ ) \qquad [3.4]$$

The $K_{c\,max}$ parameter represents the maximum ET from any cropped surface based on the amount of energy available from incoming solar radiation and is typically adjusted for relative humidity, wind speed, and crop height:

$$K_{c\,max} = \max\left(\left\{1.2 + [0.04\,(u_2 - 2) - 0.004\,(RH_{min} - 45)]\left(\frac{h}{3}\right)^{0.3}\right\}, \{K_{cb} + 0.05\}\right) \qquad [3.5]$$

The K_r coefficient modulates soil evaporation rate during the energy-limited (i.e., stage I evaporation) and water-limited (i.e., stage II evaporation) stages:

$$Kr = 1 \text{ for} \qquad De_{\,i-1} = REW \qquad [3.6a]$$

$$K_r = \frac{TEW - De_{i-1}}{TEW - REW} \qquad \text{for} \qquad De_{\,i-1} > REW \qquad [3.6b]$$

where $De_{\,i-1}$ is the depletion depth of the soil surface soil layer the previous day (mm), *TEW* is the total evaporable water of the surface evaporative layer, and *REW* is the readily evaporable water. In Eq. 3.6b, *TEW* represents the maximum possible cumulative evaporation from the soil

surface layer and *REW* represents the cumulative depth of evaporation at the end of the energy-limiting stage (mm). The *TEW* mostly depends on the soil textural class and can be estimated as:

$$TEW = 1000\ (\theta_{FC} - 0.5\ \theta_{WP})\ Z_e \quad [3.7]$$

where θ_{FC} is the volumetric soil water content at field capacity, θ_{WP} is the volumetric water content at the permanent wilting point, and Z_e is the thickness of the surface evaporative layer in meters. The soil water balance of the evaporative layer is then computed as:

$$De_i = De_{\,i-1} - (P_i - RO_i) + \frac{E_i}{f_{ew}} + DPe_i \quad [3.8]$$

where De_i and $De_{\,i-1}$ (mm) are cumulative depth of evaporation of the topsoil at the end of day *i* and *i-1*, P_i is precipitation (mm); RO_i is runoff from the soil surface (mm) determined using the curve number method (Hawkins et al., 2008), and DPe_i (mm) is deep percolation from the surface layer when soil water content exceeds field capacity. In this study, transpiration was assumed to be negligible in the surface evaporative layer.

Measurements of surface soil moisture and fraction of green canopy cover

Volumetric water content was measured at hourly intervals in the top 12 cm of the soil profile using an open-bottom instrumented microlysimeter. We selected a soil layer of 12 cm to match the thickness of the surface evaporative layer in the DualKc model, so that sensor observations could be directly assimilated into the model. The instrumented microlysimeters (12-cm length, 10-cm inner diameter) were constructed with Schedule 40 polyvinyl chloride (PVC) pipe. Each microlysimeter had one end beveled at approximately 45-degree angle to facilitate insertion into the soil and minimize soil compaction. A total of 12 microlysimeters were inserted into the soil with the help of a wooden block and an anti-vibration nylon hammer. In this particular case, the microlysimeters were not excavated and were not sealed at the bottom, which

allowed for free drainage and capillary flow in and out of the microlysimeter to maintain soil moisture conditions inside the microlysimeter volume similar to that of the surrounding soil during the entire growing season. Then, a small trench was excavated on the outside of the inserted microlysimeter to install a capacitance soil moisture sensor (model TEROS 12, METER Group Inc.). The sensor was vertically inserted, positioning the mid rod 6 cm from the soil surface, with the cable oriented upwards along the outer wall of the microlysimeter (Appendix B Figure B- 1). Each microlysimeter had three holes with a diameter slightly larger than the diameter of the sensor stainless-steel prongs (~5 mm). The epoxy head of the sensor remained outside of the microlysimeter in contact with the surrounding soil. In preliminary laboratory tests, we confirmed that the effect of the PVC wall and the sensor head being outside of the microlysimeter volume had negligible impact in the observed volumetric water content within the microlysimeter volume (Figure 3-1). The PVC wall served as an effective barrier to prevent shallow roots from entering the microlysimeter volume. This was confirmed visually at the end of the winter wheat growing seasons when the microlysimeters were removed. Thus, changes in soil moisture within the microlysimeter volume during the growing were mostly related to precipitation and soil evaporative losses. Volumetric water content inside the microlysimeters was recorded hourly and used two-fold: 1) to update the soil moisture depletion of the evaporative layer computed by the DualKc model using a direct insertion approach (see next section) and 2) as a direct method to quantify soil evaporation rate using daily changes in soil water storage (ΔS):

$$E \approx \Delta S = (\theta_t - \theta_{t-1})Z \qquad [3.9]$$

where θ_t is the volumetric water content reported by the sensor on the last hour of the day, θ_{t-1} is the volumetric water content reported by the sensor on the last hour of the previous day, and Z

is the thickness of the soil layer represented by the instrumented microlysimeter, which is the same as Z_e in the DualKc model. We installed a total of twelve TEROS 12 sensors between winter wheat rows and we also added TEROS 12 sensors outside the instrumented microlysimeters to monitor variations between the readings inside the instrumented microlysimeter and the surrounding soil.

The fraction of green canopy cover (FGCC) was estimated from downward-facing images that were collected weekly during the winter wheat growing seasons. A total of three images were collected per plot and then analyzed using the Canopeo App (Patrignani & Ochsner, 2015). In this study we assumed that the FGCC estimated from digital images is equivalent to the fraction of soil cover (i.e., f_c) in the DualKc model, which plays a pivotal role partitioning the amount of energy reaching the soil surface that is available for soil evaporation. Weekly field measurements of FGCC were linearly interpolated to generate a daily timeseries for each growing season and then these estimations were assimilated into the model using the direct insertion method.

Data assimilation of *in situ* observations

Daily average *in situ* observations of surface soil moisture from the instrumented microlysimeters and weekly observations of FGCC interpolated at daily scale were assimilated into the DualKc model using the direct insertion method. This assimilation method consists of replacing a state variable such as *De* or f_c in the model with actual sensor measurements. The assumption of the direct insertion method is that field observations have negligible uncertainty compared with the model routine simulating the same state variable, and thus, updating the state variable with *in situ* observations should increase model accuracy.

Based on the available field observations of surface soil moisture and canopy cover for the winter wheat and bare soil experiments, we tested a total of five data-driven methods to estimate soil evaporation. The first method, referred to as "DualKc" follows the standard soil water balance implementation detailed in the FAO-56 procedure using crop and soil parameters as provided in the FAO-56 tables (Table 3-1). The second method, "DualKc + FGCC", integrates observations of FGCC estimated from downward-facing images. In this method, observations of FGCC are used to replace the state variable f_c in the DualKc model with the aim of improving the partitioning of available energy reaching exposed soil. The third method, "DualKc + SSM", integrates *in situ* observations of SSM to update the depletion of the surface layer, *De*, using the direct insertion method. This method is aimed at providing model sub-routines with improved information about the available soil moisture for soil evaporation. Volumetric soil water content measured by the TEROS 12 sensor in the instrumented microlysimeter ($\theta_{\text{sensor i}}$) is converted into soil water depletion as follows:

$$De_i = TEW - 1000\left(\theta_{\text{sensor i}} - 0.5\,\theta_{wp}\right) Z_e \qquad [3.10]$$

The fourth method, "DualKc + FGCC + SSM" integrates both FGCC and SSM. The fifth method, "ΔS", is based on estimating soil evaporation solely using changes in observed soil water storage calculated with Eq. [3.9]. The second and fourth methods (i.e., those that included FGCC measurements) were only possible during the 2021/2022 and 2022/2023 winter wheat growing seasons.

Validation of soil evaporation using traditional microlysimeters

Traditional bottom-sealed microlysimeters (12 cm length, 10 cm inner diameter) constructed from PVC pipe were used to validate the different approaches for estimating soil

evaporation rate evaluated in this study. The diameter of the microlysimeters was dictated by the row spacing of the winter wheat crop, so a diameter of 10 cm allowed us to center the microlysimeters between winter wheat rows, while still maintaining a small buffer area of few centimeters to avoid damaging shallow plant roots during installation. For each field measurement during a rain-free period, a total of 12 microlysimeters (three microlysimeters in each of the four plots) were inserted into the soil and excavated, while maintaining the bore hole as intact as possible The outside wall of the microlysimeter was then cleaned and the bottom was sealed with thin nylon film and tape. After weighing the microlysimeters to determine their initial mass, they were returned to the borehole ensuring good contact with the soil. In this study we favored the use of a thin nylon film (Glad Press'n Seal Plastic Wrap) instead of a rigid PVC base to maximize the amount of heat transfer between the soil inside and below the microlysimeter (Evett et al., 1995). Microlysimeters were weighed every 24 hours either early in the morning or late in the afternoon for a period of three consecutive days, which is the typical duration for which the soil moisture within the microlysimeter remains similar to that of the surrounding soil (Daamen et at., 1993). For each measurement day, soil evaporation rate was determined as the average soil evaporation rate of the 12 microlysimeters. The performance of the different approaches for estimating soil evaporation rate were evaluated using the root mean square error (RMSE), the mean absolute error (MAE), and the Nash–Sutcliffe efficiency (NSE) coefficient.

Results and Discussion

Environmental conditions during the study period

Total precipitation for the 2021/2022 winter wheat growing season at the Ashland Bottoms Experiment Station (Figure 3-2) was 443 mm, a value that is 16% higher than the 30-year (1990-2019) precipitation for the typical winter wheat growing period in this region from mid-October to mid-June. During the same growing season, the total grass ET_o was 572 mm, which is 7% higher than the long-term average for this location. Air temperature during the 2021/2022 growing season ranged from -21℃ to 37 ℃, with a daily mean of 8.8℃, which is similar to the typical average temperature during winter wheat growing season for this region. Similarly, in the 2022/2023 growing season (Figure 3-3), the precipitation totaled 406 mm, a value 7% higher than the long-term average rainfall for the same period. During the same growing season, total grass ET_o was 546 mm, which is 2.4% higher than the long-term average for this location, and air temperature ranged between -22℃ and 34℃, with a mean air temperature for the growing season of 8.0 ℃. In the bare soil experiment during the summer of 2023 (Figure 3-4), the site received a total precipitation of 131 mm, a value 26% lower compared to the 30-year average precipitation total for the same period. The grass ET_o for the bare soil experiment in 2023 was 240 mm, which is 14% lower than the long-term average for this location. The range of temperature was between 19 ℃ and 33 ℃, with a mean equal to 26 ℃, which is only 1 ℃ higher than the long-term average daily mean air temperature for this period.

Winter wheat evaporation in a silty clay loam soil

In the winter wheat growing season of 2021/2022, the DualKc model was the most effective approach for estimating soil evaporation, with a RMSE = 0.57 mm day^{-1} (Table 3-2).

The second-best performing model in this season was the DualKc + FGCC, with RMSE = 0.68 mm day^{-1}. A comparison between the model predictions on evaporation rate and the *in situ* observation of soil evaporation for a given day revealed that the models resulting in better agreement were the DualKc and DualKc + FGCC (Table 3-2). In the subsequent winter wheat growing season of 2022/2023, the DualKc + FGCC model outperformed all the other methods, with RMSE = 0.53 mm day^{-1} (Table 3-2). The second-best model for this season was the DualKc, which had RMSE = 0.63 mm day^{-1}. Once again, upon examining the timeseries and comparing the predictions made by the models with the *in situ* observations of soil evaporation, it is evident that the models with the most robust performance are the DualKc and the DualKc + FGCC (Figure 3-3). In both winter wheat seasons, the ΔS approach consistently underperformed the other methods, with RMSE = 2.0 mm day^{-1} for the 2021/2022 season and 1.51 mm day^{-1} for the 2022/2023 growing season (Table 3-3). When comparing the timeseries of soil evaporation observations measured with the instrumented microlysimeter against those measured with the traditional microlysimeter, which serves as the ground-truth method, overestimations are notable, especially following precipitation events, as illustrated in both Figure 3-2 for winter wheat growing season 2021-2022 and Figure 3-3 for winter wheat growing season 2022-2023.

The observed volumetric water content from the TEROS 12 sensors ranged between 0.160 cm^3 cm^{-3} and 0.380 cm^3 cm^{-3} with a mean moisture of 0.255 cm^3 cm^{-3} for season 2021/2022 and ranged between 0.120 and 0.39 cm^3 cm^{-3} in 2022/2023 with a mean value of 0.223 cm^3 cm^{-3}. Thus, the observed surface soil moisture conditions during both growing seasons generally corresponded well with the range specified in the DualKc model, which uses parameters $\theta_{wp}/2$ and θ_{FC} with the range between $\theta_{wp}/2$ = 0.10 cm^3 cm^{-3} and θ_{FC} = 0.35 cm^3 cm^{-3}, although occasionally, hourly *in situ* soil moisture observations were larger than θ_{FC}. To

verify the tabulated values used to define the lower and upper soil moisture limits in the DualKc model, we collected undisturbed soil samples using 5-cm long and 5-cm diameter stainless steel rings centered at 6 cm depth to measure θ_{wp} and θ_{FC} in laboratory conditions using pressure cells (Tempe cells, Soil moisture Equipment, Inc.) set at -10 kPa and pressure plates apparatus (model 1500F2, Soil moisture Equipment, Inc.) set at -1,500 kPa, which resulted in $\theta_{WP} = 0.17$ cm^3 cm^{-3} and $\theta_{FC} = 0.31$ cm^3 cm^{-3}. To further verify the tabulated value of field capacity, θ_{FC} was estimated by averaging the volumetric water content of the twelve soil moisture sensors 24 hours after the end of a large rainfall event on 4 November 2022 totaling 72 mm, which resulted in a mean volumetric water content for the twelve TEROS 12 sensors of 0.34 cm^3 cm^{-3}. The high similarity between tabulated values and independent laboratory and field measurements provides evidence that the texture-based values in the FAO-56 manual represent good estimates of model parameters.

Based on error metrics, the DualKc alternative proved to be the most accurate method for estimating soil evaporation. Using the results from this model, we found that the total evaporation for the 2021/2022 season was 170 mm, representing 38% of the total precipitation for the growing season and 30% of the grass ET_o. In the following season winter wheat growing season of 2022/2023, total evaporation was 216 mm, representing 53% of the growing season precipitation and 40% of the grass ET_o. A prior global-scale study modeling evaporation reported values of E/ET_o around 35% and of E/P around 40% (Or & Lehman, 2019) for the U.S. Great Plains. The magnitude of E/ET_o, during the initial periods (i.e., mid-October until April), was 30% in the 2021/2022 season and 62% in the 2022/2023 season. For the 2021/2022 season, the estimated soil evaporation using DualKc was 64 mm, with an ET_o of 218 mm during that period. In contrast, for the 2022/2023 season, the soil evaporation amounted to 133 mm, while the grass

ET_o was 216 mm. During the crop development stage (i.e., April until May) the magnitude of E/ET_o resulted in 22% in the 2021/2022 season and 20% in the 2022/2023 season. In the mid-season period (i.e., May until June), E/ET_o became smaller compared to previous stages, constituting 20% for season 2021/2022 and 15% for season 2022/2023. This reduction can be attributed to the maximum ground cover during the mid-stage period, resulting in minimal energy reaching the soil surface. During the senescence period, the magnitude of E/ET_o increased to 62% in the 2021/2022 season and 36% in the 2022/2023 season. Some disparity in soil evaporation can be attributed to variations in the amount of residue between the two seasons. Furthermore, differences between years can be attributed to differences in the frequency and amount of rainfall between seasons, in the definition of the length of crop growth stages, the effective plant density, and crop growth habits that influence the shadowing of the soil surface (Zhao et al. 2013).

In the rainfed system where our study was conducted, the primary source of water input was precipitation and one possible reason for the substantial number of evaporative losses during winter wheat growing seasons could be attributed to the large number of small precipitation events during the winter wheat season that are more prone to rapid evaporation from the soil surface, crop residue, and standing vegetation. For instance, 36 out of the 51 recorded rainfall events during the 2021/2022 growing season had a magnitude <10 mm d^{-1}, constituting nearly 20% of the growing season precipitation. The following growing season 2022/2023, 47 out of 58 precipitation events were <10 mm, constituting 32% of the total precipitation for the growing season. A prior study in this region using hourly soil moisture and precipitation from May 2017 to December 2020 from the Kansas Mesonet found that rainfall events totaling <7.5 mm d^{-1} rarely infiltrate the soil beyond a 5 cm depth (Parker & Patrignani, 2021). Examining the 30-year

(1990-2019) precipitation record for this location, 74% of the daily rainfall events are smaller than <10 mm. This underscores the limited effectiveness of smaller precipitation events and the vulnerability of rainfed systems in this region to small and modest rainfall events that are prone to evaporation.

The process of evaporation relies on both the availability of soil moisture and the available energy. However, our results suggest that when estimating soil evaporation with DualKc in the context of winter wheat, the key factor to consider is the partitioning of energy rather than simply assimilating surface soil moisture (SSM). The primary input to the energy balance is solar radiation, which is greater during the initial growth stages of winter wheat but as the crop canopy progresses through its development stages, the incoming solar radiation reaching the soil surface for evaporation diminishes, consequently reducing the evaporation rate. Therefore, the gain in modeled soil evaporation accuracy when assimilating canopy cover information opens new opportunities to use proxy variables to estimate basal crop coefficients that can improve the partition of energy of simple soil water balance models. For instance, a previous study in irrigated corn with a plastic mulching found a strong (R^2 = 0.99) relationship between green canopy cover and basal crop coefficients (Ding et al., 2013). A study conducted in the vicinity of Greeley, Colorado, showed a robust linear relationship between corn FGCC and K_{cb}, a relationship that was particularly strong when the FGCC was less than 0.8 (Trout and DeJonge, 2018). In that study, FGCC for corn was assessed by utilizing a digital camera positioned 6 meters above the ground, and the images were analyzed with software to distinguish the green plant canopy from background elements, like our approach. In a study of irrigated winter wheat, Er-Raki et al. (2007) found a strong relationship (R^2 = 0.89) between the Normalized Difference Vegetation Index (NDVI), measured using a multi-spectral radiometer

(model MSR87, Cropscan Inc., USA), and the K_{cb}. The strong correlation between FGCC and NDVI offers a promising avenue for integrating readily available NDVI data from hand-held and remote sensors into the DualKc model. One possible reason for the different accuracy between the two growing seasons when estimating soil evaporation with DualKc + FGCC may be attributed to the fact that we assumed the same crop coefficients for both growing seasons. If the coefficients were adapted properly considering for example the crop density, the accuracy may be improved.

A common limitation in both the DualKc model alone and the DualKc + FGCC approach is that the depletion of the evaporative layer tends to be higher than the *in situ* depletion measured with the instrumented microlysimeter (Figure 3-2 and Figure 3-3). This implies that the model predicts faster soil drying compared to what is observed in the field. When comparing the depletion rates of DualKc, DualKc + FGCC, and DualKc + SSM, it appears that incorporating surface soil moisture (SSM) may enhance the accuracy of depletion rate estimations due to its influence on evaporation rates. A study conducted in Morocco, focusing on wheat, revealed disparities between DualKc predictions and actual evaporation from a lysimeter, and the reason for these differences was attributed to the model's tendency to predict faster soil drying compared to the observed drying in the lysimeter (Rafi et al., 2019).

Bare soil evaporation in a loam soil

In the bare soil study, the most effective method for estimating soil evaporation was the ΔS approach, with a RMSE of 0.57 mm day^{-1} (Table 3.3). Contrary to our expectations, the DualKc + SSM exhibited the poorest performance with an RMSE of 1.87 mm day^{-1}, and the DualKc alone resulted in a RMSE of 1.49 mm day^{-1} (Table 3-2). When comparing the

predictions of these approaches for soil evaporation with the in-situ observations of soil evaporation from the bare soil experiment, we noticed that the ΔS approach performed the best (Figure 3-4). We also observed a range of volumetric water content between 0.062 cm^3 cm^{-3} and 0.330 cm^3 cm^{-3} with a mean moisture of 0.124 cm^3 cm^{-3} for the summer season. For the DualKc approaches evaluated in this study, we implemented tabulated values of θ_{FC} = 0.25 cm^3 cm^{-3} and θ_{WP} = 0.12 cm^3 cm^{-3} as inputs for DualKc models, we also conducted a laboratory experiment employing pressure cells set at -10 kPa resulting in θ_{FC} = 0.25 cm^3 cm^{-3} and pressure plates apparatus set at -1,500 kPa resulting in θ_{WP} = 0.07 cm^3 cm^{-3}. For further verification of the tabulated values, we compare the average of three TEROS 12 sensor readings after the end of a large precipitation event on 4-5 July, resulting in a volumetric water content of 0.26 cm^3 cm^{-3}.

The ΔS approach exhibited unusually high soil evaporation rates, which were an artifact of large changes in soil water storage resulting from drainage rather than evaporative losses (Figure 3-4). To mitigate the influence of drainage in the ΔS approach, a straightforward solution involves ignoring volumetric water content from the sensor exceeding θ_{FC}, under the assumption that any water content exceeding θ_{FC} corresponds to drainage. A more robust solution to this problem could be the integration of *in situ* observations with a numerical model such as HYDRUS (Šimůnek et al., 2006); however, this alternative would require additional soil physical properties to accurately estimate soil water dynamics. A promising alternative to integrate *in situ* observations of soil moisture with a modeling framework is to use the surface evaporative capacitance (SEC) method, which simulates surface soil moisture as a capacitor that is filled by precipitation and is emptied by both drainage and soil evaporation (Or and Lehmann, 2019). Thus, *in situ* soil moisture data can offer insights into the current state of this "capacitor," potentially enhancing soil evaporation estimates. Even machine learning models could be the key

to reconcile multiple soil evaporation methods into a new data-driven technique for *in situ* soil evaporation measurements by integrating relevant data such as precipitation, soil properties, and environmental conditions. Machine learning models can capture more complex and non-linear relationships between variables after being trained with data from different scenarios that could be derived from laboratory, greenhouse, and field experiments.

The ΔS is an approach for *in situ* quantification of soil evaporation, however the implementation of the instrumented microlysimeter in this approach has limitations. For example, when assessing the volumetric water content within the TEROS 12 inside the instrumented microlysimeter and the values recorded by a TEROS 12 sensor outside, but nearby, the microlysimeter, we observed an RMSE of 0.04 $cm^3\ cm^{-3}$ and an MAE of 0.032 $cm^3\ cm^{-3}$ between sensors. At the beginning of the growing season, the observed water content showed little variation between the measurements obtained from the sensor inside the microlysimeter and the sensor positioned outside the microlysimeter in the row. However, as winter wheat began to grow, the differences in volumetric water content increased due to the crop's growth and elevated water uptake. The difference in soil temperature measured inside the instrumented microlysimeter and in the soil yielded an RMSE = 4 ˚C and MAE = 3 ˚C, and the temperature inside the instrumented microlysimeter was cooler (Figure 3-5). One reason for this may be that the low thermal conductivity of the PVC has some insulating effect reducing the heat transfer between the soil inside the microlysimeter and the surrounding soil that was not expected. Additionally, the presence of PVC in contact with the TEROS 12 sensor rods, as part of the instrumented microlysimeter set up, may have contributed to these discrepancies in volumetric water content and temperature measurements, during a laboratory calibration we found that the

measurements with rods embedded in the PVC are unbiased, with RMSE of 0.014 cm^3 cm^{-3} (Figure 3-1).

There are other challenges associated with adopting the ΔS approach to estimate soil evaporation rate, these include the relatively small volume of soil sampled and the potential for deep percolation losses or gains through capillary rise that can be minimized with some models (Allen et al., 2011). Furthermore, this approach requires ignoring days when air temperatures fell below 1˚C due to changes in the apparent dielectric permittivity of partially frozen soils, which can impact the estimation of volumetric water content (Seyfried and Grant, 2007; Parker and Patrignani, 2021), and consequently affect ΔS estimations. The primary limitation of this study lies in the validation method. Although traditional microlysimeters proved valuable for evaluating data-driven and model-based approaches, they have limitations in terms of continuous soil evaporation monitoring and spatial representativeness. To enhance future validation efforts, the use of automated weighing microlysimeters similar to that proposed by Rumana (2015) could be considered.

Data driven approach based on soil evaporation reduction coefficient

Contrary to our expectations that surface soil moisture may improve the estimation of soil evaporation by assimilating continuous and accurate data measured with a soil moisture sensor, the DualKc + SSM resulted to be the worst approach across the three experiments (Figure 3-5). One possible explanation for this may be the oversimplified linear relationship between surface soil moisture and evaporation in the DualKc model. The standard method described in the FAO-56 manual (Allen et al., 1998) provides a simple linear relationship between soil moisture and soil evaporation rate, but new studies have shown that soil texture-based representations of the

actual and potential soil evaporation rate as a function of surface soil moisture can result in more accurate estimation of soil evaporation rate compared with the standard *ad hoc* approach described in the FAO-56 manual (Merlin et al., 2016; Amazirh et al., 2021). The expression proposed for the texture-base K_r for various soil layers thickness is expressed as:

$$K_r = \left[0.5 - 0.5\ \cos\left(\pi \frac{\theta_L}{\theta_{max}}\right)\right]^P \qquad [3.11]$$

whit θ_L represents the water content in a soil layer with a thickness denoted as *L*, where *L* can have any arbitrary value up to 100 cm, and θ_{max} being the soil moisture at saturation, and *P* is a function dependent on both *L* and potential soil evaporation (Merlin et al., 2011). To assess the effectiveness of this approach within our study, we applied a data drive approach, utilizing the formulation proposed by Merlin et al. (2011) for the DualKc model:

$$K_r = \left[0.5 - 0.5\ \cos\left(\pi \frac{\theta_{sensor}}{\theta_{FC}}\right)\right]^P \qquad [3.12]$$

where θ_{sensor} is the volumetric water content measured *in situ* with instrumented microlysimeters extending to a depth of 12 cm. Since this relationship modulates the soil evaporation rate of the wetted and exposed soil, the optimal parameter *P* for the two winter wheat seasons was obtained using a quantile regression analysis by fitting the model to the 0.95 quantile of the observed changes in soil water storage from the instrumented microlysimeters as a function of E/E_p (E is the soil evaporation and E_p is the potential soil evaporation) (Figure 3-7), where E_p was defined as $1.2\ ET_o$, which is similar to the representation of maximum available energy for soil evaporation in the DualKc model (i.e., $K_{c\ max}$). We did not apply any optimization for the bare soil approach since the soil remained exposed throughout the entire period. The main advantage of data-driven approach based on soil evaporation reduction coefficient is that it simplifies the steps of the DualKc and the data assimilation approaches. With the surface soil moisture

observations from instrumented microlysimeter K_r [Eq.12] is estimated and soil evaporation can be predicted with the following equation:

$$E = ET_o\, K_r\, (K_{c\,max} - K_{cb}) \quad [3.13]$$

Our findings demonstrated an improvement when incorporating a non-linear model based on surface soil moisture observations for both the DualKc + SSM and DualKc + FGCC + SSM approaches in both winter wheat growing seasons (Figure 3-8). We observed a substantial reduction in the error ranging from 25% to about 40% when K_r is estimated based on Eq. 12, resulting in RMSE < 0.65 mm day^{-1} (Table 3.4). In the bare soil experiment, we noted substantial improvements with errors in daily soil evaporation rate decreasing by about 30% compared to the linear -plateau model proposed by Allen et al., (1998) (Table 3-4).

We compared the slopes of the linear model (Allen et al., 1998) and fitted K_r (Figure 3-7), resulting in a slope of 5.91 (unitless) for the DualKc model and a slope of 5.25 for our non-linear approach based on *in situ* observations of surface soil moisture. In the bare soil study, the fitted model resulted in a slope of 10.9, whereas the DualKc model yielded a slope of 8.7. The behavior of the two approaches differs for both winter wheat and bare soil. The curve generated by the Merlin et al. (2011) model exhibited a less steep slope, indicating that variations in soil moisture might have a limited impact on K_r, meaning a weaker relationship between the two variables.

The fitted non-linear soil evaporation reduction coefficient model, which was derived from hourly *in situ* observations of SSM using an instrumented microlysimeter, offers a valuable alternative for developing data-driven approaches. Possibly, the sensor failed to capture the initial change in soil moisture at the immediate soil surface, potentially resulting in an inaccurate estimation of soil moisture and affecting the performance of prior approaches. In future studies

the instrumented microlysimeter setting should be re-considered, exploring modifications to more effectively capture changes in the topmost soil layer. Furthermore, undertaking field calibrations is essential to deepen our comprehension of potential limitations and to guarantee the precision of soil moisture measurements. Although the DualKc model is relatively simple, it outperforms all the tested approaches. This highlights the importance of prioritizing accurate parameterization to better reflect field conditions, rather than relying solely on general or scientifically reported soil parameters (Mutziger et al., 2005).

Conclusions

- The FAO-56 Dual Crop Coefficient is a simple model that, when properly parameterized, provides reliable estimation of soil evaporation rate, and a model-data assimilation approach using this model proved effective in generating daily estimates of soil evaporation rate over the entire growing season.
- The assimilation of FGCC within the DualKc model resulted in an accurate estimation of surface soil evaporation in winter wheat with RMSE = 0.6 mm day^{-1}. Our findings suggest that improving the partitioning of available energy at the soil surface seems to be more important than improving the available moisture for accurate estimations of soil evaporation. Thus, there exists an opportunity for using time-lapse photography and high-resolution remote sensing technologies to better model soil evaporation dynamics.
- Contrary to our initial expectations, estimation of soil evaporation based on changes in surface soil water storage using an open-bottom instrumented microlysimeter resulted in reasonable estimates of soil evaporation rates in bare soil but had poor performance in winter wheat experiments.

- The non-linear soil evaporation reduction factor, which correlates observed changes in soil water storage as a function of E/Ep, improves the accuracy of soil evaporation estimates in winter wheat to RMSE<0.65 mm day^{-1} and in bare soil to RMSE≤0.80 mm day^{-1}. The main advantage of this approach is its practical field implementation and the simplicity of the model, which only requires estimates of $K_{c\ max}$, K_{cb}, and ET_o.
- The instrumented microlysimeter may have failed to capture the variations in soil moisture changes at the immediate soil surface (top 1 cm), potentially resulting in an inaccurate estimation of soil moisture in the layer undergoing soil evaporation.

References

Amazirh, A., Merlin, O., Er-Raki, S., Bouras, E., & Chehbouni, A. (2021). Implementing a new texture-based soil evaporation reduction coefficient in the FAO dual crop coefficient method. *Agricultural Water Management*, *250*, 106827. https://doi.org/10.1016/j.agwat.2021.106827

Allen, R. G., Pereira, L. S., Raes, D., & Smith, M. (1998). Crop evapotranspiration-Guidelines for computing crop water requirements-FAO Irrigation and drainage paper 56. Fao, Rome, 300(9), D05109.

Allen, R. G., Smith, M., Pereira, L. S., Raes, D., & Wright, J. L. (2000). Revised FAO procedures for calculating evapotranspiration: irrigation and drainage paper no. 56 with testing in Idaho. In Watershed Management and Operations Management 2000 (pp. 1-10).

Allen, R. G., Pruitt, W. O., Raes, D., Smith, M., & Pereira, L. S. (2005). Estimating evaporation from bare soil and the crop coefficient for the initial period using common soils information. *Journal of irrigation and drainage engineering*, 131(1), 14-23. https://doi.org/10.1061/(ASCE)0733-9437(2005)131:1(14)

Allen, R. G., Pereira, L. S., Howell, T. A., & Jensen, M. E. (2011). Evapotranspiration information reporting: I. Factors governing measurement accuracy. *Agricultural Water Management*, *98*(6), 899-920. https://doi.org/10.1016/j.agwat.2010.12.015

Baker, J. M., & Spaans, G. J. (1994). Measuring water exchange between soil and atmosphere with TDR-microlysimetry. *Soil science*, 158(1), 22-30. https://doi.org/10.1097/00010694-199407000-00003

Berg, A., & Sheffield, J. (2019). Evapotranspiration partitioning in CMIP5 models: uncertainties and future projections. *Journal of Climate*, 32(10), 2653-2671. https://doi.org/10.1175/JCLI-D-18-0583.1

Boast, C. W., & Robertson, T. M. (1982). A "micro-lysimeter" method for determining evaporation from bare soil: description and laboratory evaluation. *Soil Science Society of America Journal*, *46*(4), 689-696. https://doi.org/10.2136/sssaj1982.03615995004600040005x

Bristow, K. L., Kluitenberg, G. J., & Horton, R. (1994). Measurement of soil thermal properties with a dual-probe heat-pulse technique. *Soil Science Society of America Journal*, 58(5), 1288-1294. https://doi.org/10.2136/sssaj1994.03615995005800050002x

Dane, J. H., & Hopmans, J. W. 3.3.2 Laboratory. 675-720. https://doi.org/10.2136/sssabookser5.4.c25

Ding, R., Kang, S., Zhang, Y., Hao, X., Tong, L., & Du, T. (2013). Partitioning evapotranspiration into soil evaporation and transpiration using a modified dual crop coefficient model in irrigated maize field with ground-mulching. *Agricultural Water Management*, *127*, 85-96. https://doi.org/10.1016/j.agwat.2013.05.018

Er-Raki, S., Chehbouni, A., Guemouria, N., Duchemin, B., Ezzahar, J., & Hadria, R. (2007). Combining FAO-56 model and ground-based remote sensing to estimate water consumptions of wheat crops in a semi-arid region. *Agricultural Water Management*, *87*(1), 41-54. https://doi.org/10.1016/j.agwat.2006.02.004

Er-Raki, S., Ezzahar, J., Merlin, O., Amazirh, A., Hssaine, B. A., Kharrou, M., Khabba, S., & Chehbouni, A. (2021). Performance of the HYDRUS-1D model for water balance components assessment of irrigated winter wheat under different water managements in

semi-arid region of Morocco. *Agricultural Water Management*, 244, 106546. https://doi.org/10.1016/j.agwat.2020.106546

Evett, S. R., Warrick, A. W., & Matthias, A. D. (1995). Wall material and capping effects on microlysimeter temperatures and evaporation. *Soil Science Society of America Journal*, *59*(2), 329-336. https://doi.org/10.2136/sssaj1995.03615995005900020009x

Evett, S. R., Tolk, J. A., & Howell, T. A. (2006). Soil profile water content determination: Sensor accuracy, axial response, calibration, temperature dependence, and precision. *Vadose Zone Journal*, 5(3), 894-907. https://doi.org/10.2136/vzj2005.0149.

Flumignan, D. L., Faria, R. T. D., & Lena, B. P. (2012). Test of a microlysimeter for measurement of soil evaporation. *Engenharia Agrícola*, 32, 80-90. https://doi.org/10.1590/S0100-69162012000100009

Gavlak, R., Horneck, R., & Miller, R. O. (2005). Particle size analysis: Hydrometer method.

Gee, G. W., & Bauder, J. W. (1979). Particle size analysis by hydrometer: a simplified method for routine textural analysis and a sensitivity test of measurement parameters. *Soil Science Society of America Journal*, 43(5), 1004-1007. https://doi.org/10.2136/sssaj1979.03615995004300050038x

Hawkins, R. H., Ward, T. J., Woodward, D. E., & Van Mullem, J. A. (Eds.). (2008, November). Curve number hydrology: State of the practice. *American Society of Civil Engineers*.

Jara, J., Stockle, C. O., & Kjelgaard, J. (1998). Measurement of evapotranspiration and its components in a corn (Zea Mays L.) field. *Agricultural and Forest Meteorology*, *92*(2), 131-145. https://doi.org/10.1016/S0168-1923(98)00083-5

Kizito, F., Campbell, C., Campbell, G., Cobos, D., Teare, B., Carter, B., & Hopmans, J. (2008). Frequency, electrical conductivity and temperature analysis of a low-cost capacitance soil

moisture sensor. *Journal of Hydrology*, *352*(3-4), 367-378. https://doi.org/10.1016/j.jhydrol.2008.01.021

Klocke, N. L., Todd, R. W., & Schneekloth, J. P. (1996). Soil water evaporation in irrigated corn. *Applied Engineering in Agriculture*, 12(3), 301-306. https://doi.org/10.13031/2013.25652

Kool, D., Kustas, W., Ben-Gal, A., Lazarovitch, N., Heitman, J., Sauer, T., & Agam, N. (2016). Energy and evapotranspiration partitioning in a desert vineyard. *Agricultural and Forest Meteorology*, *218-219*, 277-287. https://doi.org/10.1016/j.agrformet.2016.01.002

Lascano, R. J., Hatfield, J. L., & Upchurch, D. R. (1987). Energy and water balance of a sparse crop: Simulated and measured soil and crop evaporation. *Soil Science Society of America Journal*, *51*(5), 1113-1121. https://doi.org/10.2136/sssaj1987.03615995005100050004x

Lawrence, D. M., Thornton, P. E., Oleson, K. W., & Bonan, G. B. (2007). The partitioning of evapotranspiration into transpiration, soil evaporation, and canopy evaporation in a GCM: Impacts on land–atmosphere interaction. *Journal of Hydrometeorology*, 8(4), 862-880. https://doi.org/10.1175/JHM596.1

Lee, T. J., & Pielke, R. A. (1992). Estimating the soil surface specific humidity. *Journal of Applied Meteorology and Climatology*, 31(5), 480-484. https://doi.org/10.1175/1520-0450(1992)031<0480:ETSSSH>2.0.CO;2

Louis Baumhardt, R., & Salinas-Garcia, J. (2006). Dryland agriculture in Mexico and the US Southern Great Plains. *Dryland agriculture*, 23, 341-364. https://doi.org/10.2134/agronmonogr23.2ed.c10

Manabe, S. (1969). Climate and the ocean circulation: I. The atmospheric circulation and the hydrology of the earth's surface. *Monthly weather review*, 97(11), 739-774. https://doi.org/10.1175/1520-0493(1969)097<0739:CATOC>2.3.CO;2.

Merlin, O., Al Bitar, A., Rivalland, V., Béziat, P., Ceschia, E., & Dedieu, G. (2011). An analytical model of evaporation efficiency for unsaturated soil surfaces with an arbitrary thickness. *Journal of Applied Meteorology and Climatology*, 50(2), 457-471. https://doi.org/10.1175/2010JAMC2418.1

Merlin, O., Stefan, V. G., Amazirh, A., Chanzy, A., Ceschia, E., Er-Raki, S., Gentine, P., Tallec, T., Ezzahar, J., Bircher, S., Beringer, J., & Khabba, S. (2016). Modeling soil evaporation efficiency in a range of soil and atmospheric conditions using a meta-analysis approach. *Water Resources Research*, *52*(5), 3663-3684. https://doi.org/10.1002/2015WR018233

Metzger, J. C., Landschreiber, L., Gröngröft, A., & Eschenbach, A. (2014). Soil evaporation under different types of land use in Southern African Savanna ecosystems. *Journal of Plant Nutrition and Soil Science*, *177*(3), 468-475. https://doi.org/10.1002/jpln.201300257

Mutziger, A. J., Burt, C. M., Howes, D. J., & Allen, R. G. (2005). Comparison of measured and FAO-56 modeled evaporation from bare soil. *Journal of irrigation and drainage engineering*, 131(1), 59-72. https://doi.org/10.1061/(ASCE)0733-9437(2005)131:1(59)

Nahitiya, D., Bisheh, M. N., Lollato, R. P., & Patrignani, A. (2021). Preliminary classification of soil, plant, and residue cover using convolutional neural networks. *Kansas Agricultural Experiment Station Research Reports*, 7(5), 11. https://doi.org/10.4148/2378-5977.8081

Oleson, K. W., Lawrence, D. M., Bonan, G. B., Drewniak, B., Huang, M., Koven, C. D., ... & Yang, Z. L. (2010). Technical description of version 4.0 of the Community Land Model (CLM). NCAR Tech. Note NCAR/TN-478+ STR, 257, 1-257.

Or, D., & Lehmann, P. (2019). Surface evaporative capacitance: How soil type and rainfall characteristics affect global-scale surface evaporation. *Water Resources Research*, *55*(1), 519-539. https://doi.org/10.1029/2018WR024050

Parker, Nathaniel, and Andres Patrignani. Reconstructing precipitation events using collocated soil moisture information. *Journal of Hydrometeorology*, 22.12 (2021): 3275-3290. https://doi.org/10.1175/JHM-D-21-0168.1

Paruelo, J., Aguiar, M., & Golluscio, R. (1991). Evaporation estimates in arid environments: An evaluation of some methods for the Patagonian steppe. *Agricultural and Forest Meteorology*, *55*(1-2), 127-132. https://doi.org/10.1016/0168-1923(91)90026-M

Patrignani, A., Lollato, R. P., Ochsner, T. E., Godsey, C. B., & Edwards, J. T. (2014). Yield gap and production gap of rainfed winter wheat in the Southern Great Plains. *Agronomy Journal*, 106(4), 1329-1339. https://doi.org/10.2134/agronj14.0011.

Patrignani, A., & Ochsner, T. E. (2015). Canopeo: A powerful new tool for measuring fractional green canopy cover. *Agronomy Journal*, 107(6), 2312-2320. https://doi.org/10.2134/agronj15.0150

Pereira, L., Paredes, P., Melton, F., Johnson, L., Wang, T., López-Urrea, R., Cancela, J., & Allen, R. (2020). Prediction of crop coefficients from fraction of ground cover and height. Background and validation using ground and remote sensing data. *Agricultural Water Management*, 241, 106197. https://doi.org/10.1016/j.agwat.2020.106197

Rafi, Z., Merlin, O., Le Dantec, V., Khabba, S., Mordelet, P., Er-Raki, S., Amazirh, A., Olivera-Guerra, L., Ait Hssaine, B., Simonneaux, V., Ezzahar, J., & Ferrer, F. (2019). Partitioning evapotranspiration of a drip-irrigated wheat crop: Inter-comparing eddy covariance-, sap flow-, lysimeter- and FAO-based methods. *Agricultural and Forest Meteorology*, *265*, 310-326. https://doi.org/10.1016/j.agrformet.2018.11.031

Ritchie, J. T. (1972). Model for predicting evaporation from a row crop with incomplete cover. *Water Resources Research*, *8*(5), 1204-1213. https://doi.org/10.1029/WR008i005p01204

Ritchie, J. T., Porter, C. H., Judge, J., Jones, J. W., & Suleiman, A. A. (2009). Extension of an existing model for soil water evaporation and redistribution under high water content conditions. *Soil Science Society of America Journal*, *73*(3), 792-801. https://doi.org/10.2136/sssaj2007.0325

Robock, A., Vinnikov, K. Y., Schlosser, C. A., Speranskaya, N. A., & Xue, Y. (1995). Use of midlatitude soil moisture and meteorological observations to validate soil moisture simulations with biosphere and bucket models. *Journal of Climate*, 8(1), 15-35. https://doi.org/10.1175/1520-0442(1995)008<0015:UOMSMA>2.0.CO;2

Scott, B. L., Ochsner, T. E., Illston, B. G., Fiebrich, C. A., Basara, J. B., & Sutherland, A. J. (2013). New soil property database improves Oklahoma Mesonet soil moisture estimates. *Journal of Atmospheric and Oceanic Technology*, 30(11), 2585-2595. https://doi.org/10.1175/JTECH-D-13-00084.1

Seyfried, M. S., & Grant, L. E. (2007). Temperature effects on soil dielectric properties measured at 50 MHz. *Vadose Zone Journal*, 6(4), 759-765. https://doi.org/10.2136/vzj2006.0188

Šimůnek, J. I. R. K. A., Van Genuchten, M. T., & Šejna, M. (2006). The HYDRUS software package for simulating two-and three-dimensional movement of water, heat, and multiple solutes in variably-saturated media. Technical manual, version, 1, 241.

Šimůnek, J., Van Genuchten, M. T., & Šejna, M. (2016). Recent developments and applications of the HYDRUS computer software packages. *Vadose Zone Journal*, 15(7), https://doi.org/10.2136/vzj2016.04.0033.

Trout, T. J., & DeJonge, K. C. (2018). Crop water use and crop coefficients of maize in the great plains. *Journal of Irrigation and Drainage Engineering*, 144(6), 04018009. https://doi.org/10.1061/(ASCE)IR.1943-4774.0001309

Villalobos, F. J., & Fereres, E. (1990). Evaporation measurements beneath corn, cotton, and sunflower canopies. *Agronomy Journal*, *82*(6), 1153-1159. https://doi.org/10.2134/agronj1990.00021962008200060026x

Villegas, J. C., Espeleta, J. E., Morrison, C. T., Breshears, D. D., & Huxman, T. E. (2014). Factoring in canopy cover heterogeneity on evapotranspiration partitioning: Beyond big-leaf surface homogeneity assumptions. *Journal of Soil and Water Conservation*, 69(3), 78A-83A. https://doi.org/10.2489/jswc.69.3.78A

Trambouze, W., Bertuzzi, P., & Voltz, M. (1998). Comparison of methods for estimating actual evapotranspiration in a row-cropped vineyard. *Agricultural and Forest Meteorology*, *91*(3-4), 193-208. https://doi.org/10.1016/S0168-1923(98)00072-0

Wagle, P., Skaggs, T. H., Gowda, P. H., Northup, B. K., & Neel, J. P. (2020). Flux variance similarity-based partitioning of evapotranspiration over a rainfed alfalfa field using high frequency eddy covariance data. *Agricultural and Forest Meteorology*, *285-286*, 107907. https://doi.org/10.1016/j.agrformet.2020.107907

Wang, L., Good, S. P., Caylor, K. K., & Cernusak, L. A. (2012). Direct quantification of leaf transpiration isotopic composition. *Agricultural and Forest Meteorology*, 154, 127-135. https://doi.org/10.1016/j.agrformet.2011.10.018

Wang, L., Caylor, K. K., Villegas, J. C., Barron-Gafford, G. A., Breshears, D. D., & Huxman, T. E. (2010). Partitioning evapotranspiration across gradients of woody plant cover: Assessment of a stable isotope technique. *Geophysical Research Letters*, *37*(9). https://doi.org/10.1029/2010GL043228

Warren, J. G., Ochsner, T. E., & Godsey, C. B. (2009). Fate of precipitation falling on Oklahoma cropland. *Oklahoma Cooperative Extension Service*.

Zhao, N., Liu, Y., Cai, J., Paredes, P., Rosa, R. D., & Pereira, L. S. (2013). Dual crop coefficient modelling applied to the winter wheat–summer maize crop sequence in North China Plain: Basal crop coefficients and soil evaporation component. *Agricultural Water Management*, *117*, 93-105. https://doi.org/10.1016/j.agwat.2012.11.008

Zhao, P., Kang, S., Li, S., Ding, R., Tong, L., & Du, T. (2018). Seasonal variations in vineyard ET partitioning and dual crop coefficients correlate with canopy development and surface soil moisture. *Agricultural Water Management*, *197*, 19-33. https://doi.org/10.1016/j.agwat.2017.11.004

Zhou, S., Yu, B., Zhang, Y., Huang, Y., & Wang, G. (2016). Partitioning evapotranspiration based on the concept of underlying water use efficiency. *Water Resources Research*, *52*(2), 1160-1175. https://doi.org/10.1002/2015WR017766

Table 3-1 Parameters of the FAO-56 Dual Crop Coefficient model for winter wheat in Ashland Bottoms, Kansas including management variables, soil variables, and crop variables volumetric water content at field capacity (θ_{FC}), volumetric water content at permanent wilting point (θ_{WP}), layer thickness (Z_e), readily evaporable water (REW), basal crop coefficient at initial stages (K_{cb} Ini), mid stages (K_{cb} Mid) and end stages (K_{cb} End).

Parameter†	Winter wheat	Winter wheat	Bare soil	Source
Season	2021/2022	2022/2023	2023	
Latitude	39.00	39.00	39.14	
Altitude (m)	325	325	325	
Start date	22 Oct 2021	15 Oct 2022	23 June 2023	
End date	14 June 2022	13 June 2023	8 August 2023	
Residue cover (%)	50	40	0	Nahitiya et al., 2021
Curve number	80	80	63	Hawkins et al., 2008
θ_{FC} (cm^3 cm^{-3})	0.34	0.34	0.25	Allen et al., 1998 (Table 18)
θ_{WP} (cm^3 cm^{-3})	0.20	0.20	0.12	Allen et al., 1998 (Table 18)
Z_e (m)	0.12	0.12	0.12	
REW	12	12	20	Allen et al., 1998 (Table 18)
K_{cb} Ini	0.20	0.20	0.15	Allen et al., 1998 (Table 17)
K_{cb} Mid	0.95	0.95	0.15	Allen et al., 1998 (Table 17)
K_{cb} End	0.15	0.15	0.15	Allen et al., 1998 (Table 17)
Initial stage (days)	150	160	47	
Development stage (days)	40	40	-	
Middle stage (days)	30	20	-	
Late stage (days)	15	15	-	

Table 3-2 Error Metrics for FAO-56 Dual Crop Coefficient (DualKc), DualKc assimilation the fraction of green canopy cover (DualKc +FGCC), DualKc assimilating surface soil moisture (DualKc + SSM) and DualKc assimilation both fraction of green canopy cover and surface soil moisture (DualKc + FGCC + SSM) approaches: Mean Absolute Error (MAE), Root Mean Square Error (RMSE), and Nash–Sutcliffe Model Efficiency Coefficient (NSE) comparing *in situ* soil evaporation observations.

Land cover	**Season**	**Model**	**RMSE** mm day^{-1}	**MAE** mm day^{-1}	**NSE**
Wheat	2021/2022	DualKc	0.57	0.41	0.31
Wheat	2021/2022	DualKc + FGCC	0.68	0.47	0.04
Wheat	2021/2022	DualKc + SSM	1.03	0.68	-1.19
Wheat	2021/2022	DualKc + FGCC + SSM	1.01	0.65	-1.14
Wheat	2022/2023	DualKc	0.63	0.48	0.50
Wheat	2022/2023	DualKc + FGCC	0.53	0.44	0.64
Wheat	2022/2023	DualKc + SSM	1.13	0.94	-0.60
Wheat	2022/2023	DualKc + FGCC + SSM	1.10	0.92	-0.51
Bare soil	2023	DualKc	1.49	1.02	-0.31
Bare soil	2023	DualKc+ SSM	1.87	1.59	-1.07

Table 3-3 Table showing the mean absolute error (MAE), root mean square error (RMSE), and Nash–Sutcliffe model efficiency coefficient (NSE) between the observed soil evaporation measured with traditional microlysimeters and estimated by the change in surface (12 cm) soil water storage (ΔS) approach.

Land cover	**Season**	**Model**	**RMSE** mm day^{-1}	**MAE** mm day^{-1}	**NSE**
Wheat	2021/2022	ΔS	2.0	1.38	-3.82
Wheat	2022/2023	ΔS	1.51	0.89	-2.3
Bare soil	2023	ΔS	0.57	0.37	0.81

Table 3-4 Error Metrics for non-linear approaches: Mean Absolute Error (MAE), Root Mean Square Error (RMSE), and Nash–Sutcliffe Model Efficiency Coefficient (NSE) comparing *in situ* soil evaporation observations and the data-drive approach fitting *Kr* soil evaporation estimations. K_r represents soil evaporation reduction coefficient. FGCC is the fraction of green canopy cover simulated by FAO-56 Dual Crop Coefficient or derived from *in situ* observations.

Land cover	**Season**	**Model**	K_r	**RMSE** mm day^{-1}	**MAE** mm day^{-1}	**NSE**
Wheat	2021/2022	DualKc	Fitted	0.58	0.41	0.29
Wheat	2021/2022	DualKc + FGCC	Fitted	0.71	0.51	-0.04
Wheat	2021/2022	DualKc + SSM	Fitted	0.73	0.47	-0.12
Wheat	2021/2022	DualKc + FGCC + SSM	Fitted	0.74	0.47	-0.12
Wheat	2022/2023	DualKc	Fitted	0.68	0.52	0.42
Wheat	2022/2023	DualKc + FGCC	Fitted	0.68	0.49	0.42
Wheat	2022/2023	DualKc + SSM	Fitted	0.83	0.63	0.15
Wheat	2022/2023	DualKc + FGCC + SSM	Fitted	0.83	0.63	0.15
Bare soil	2023	DualKc	Fitted	1.26	0.80	0.07
Bare soil	2023	DualKc+ SSM	Fitted	1.1	0.66	0.28

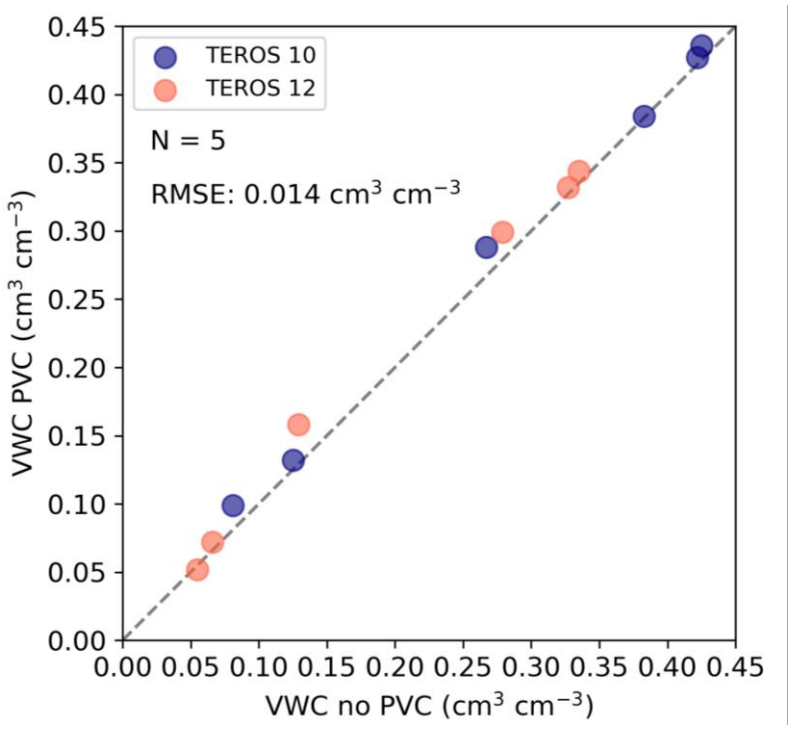

Figure 3-1. Relationship between the volumetric water content (VWC) measured with the TEROS 10 and TEROS 12 soil moisture sensors with and without a PVC layer, similar to the instrumented microlysimeter setup. *N* represents the number of observations for each sensor and *RMSE* represents the root means square error.

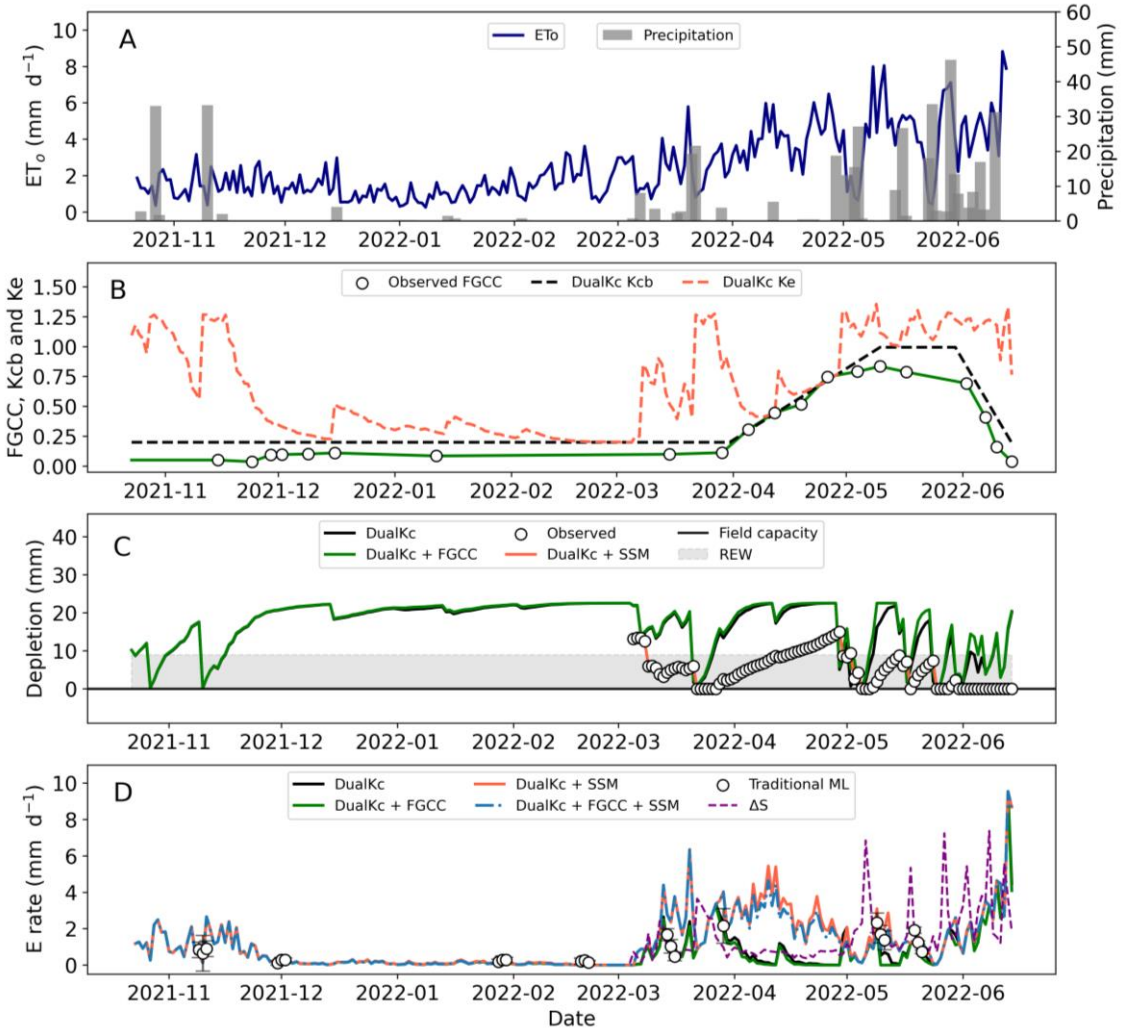

Figure 3-2. (A) Daily reference evapotranspiration (ET_o) and precipitation obtained from the Ashland Bottoms station of the Kansas Mesonet for the 2021/2022 winter wheat growing season. (B) Crop basal coefficient (K_{cb}) estimated using the Dual Crop Coefficient model (DualKc) and from observations of the fraction of green canopy cover (FGCC). (C) Depletion of the surface layer estimated by the DualKc, DualKc + FGCC, DualKc assimilating surface soil moisture (SSM) (DualKc + SSM), and the observed values of SSM. The grey band represents the ready evaporable water (REW) and the black line represents the field capacity (FC). (D) Soil evaporation rate predicted with the DualKc, DualKc + FGCC, DualKc + SSM, DualKc + FGCC + SSM, and traditional microlysimeters (ML).

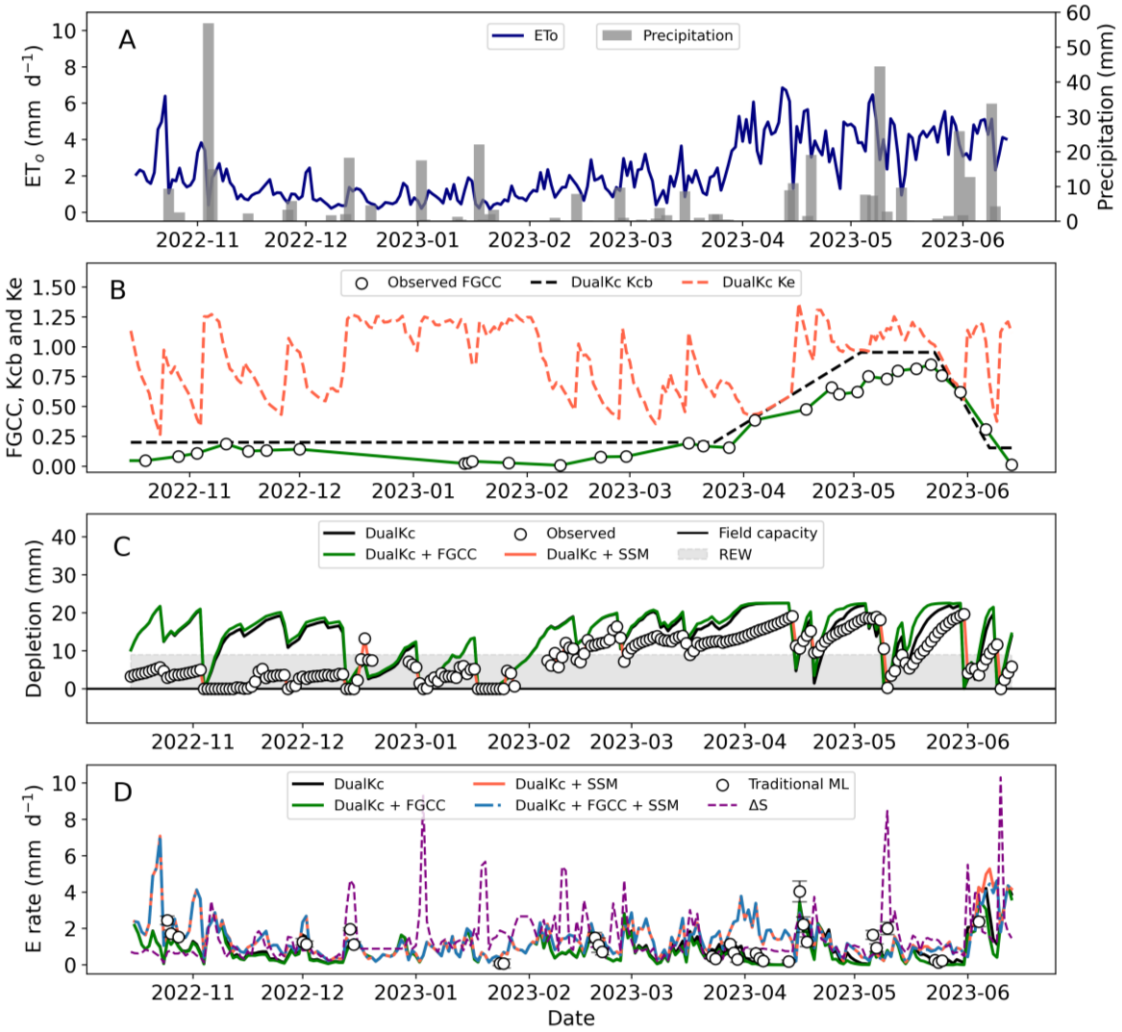

Figure 3-3 (A) Daily reference evapotranspiration (ET_o) and precipitation obtained from the Ashland Bottoms station of the Kansas Mesonet for the 2022/2023 winter wheat growing season. (B) Crop basal coefficient (K_{cb}) estimated using the Dual Crop Coefficient model (DualKc) and from observations of the fraction of green canopy cover (FGCC). (C) Depletion of the surface layer estimated by the DualKc, DualKc + FGCC, DualKc assimilating surface soil moisture (SSM) (DualKc + SSM), and the observed values of SSM. The grey band represents the ready evaporable water (REW) and the black line represents the field capacity (FC). (D) Soil evaporation rate predicted with the DualKc, DualKc + FGCC, DualKc + SSM, DualKc + FGCC + SSM, and traditional microlysimeters (ML).

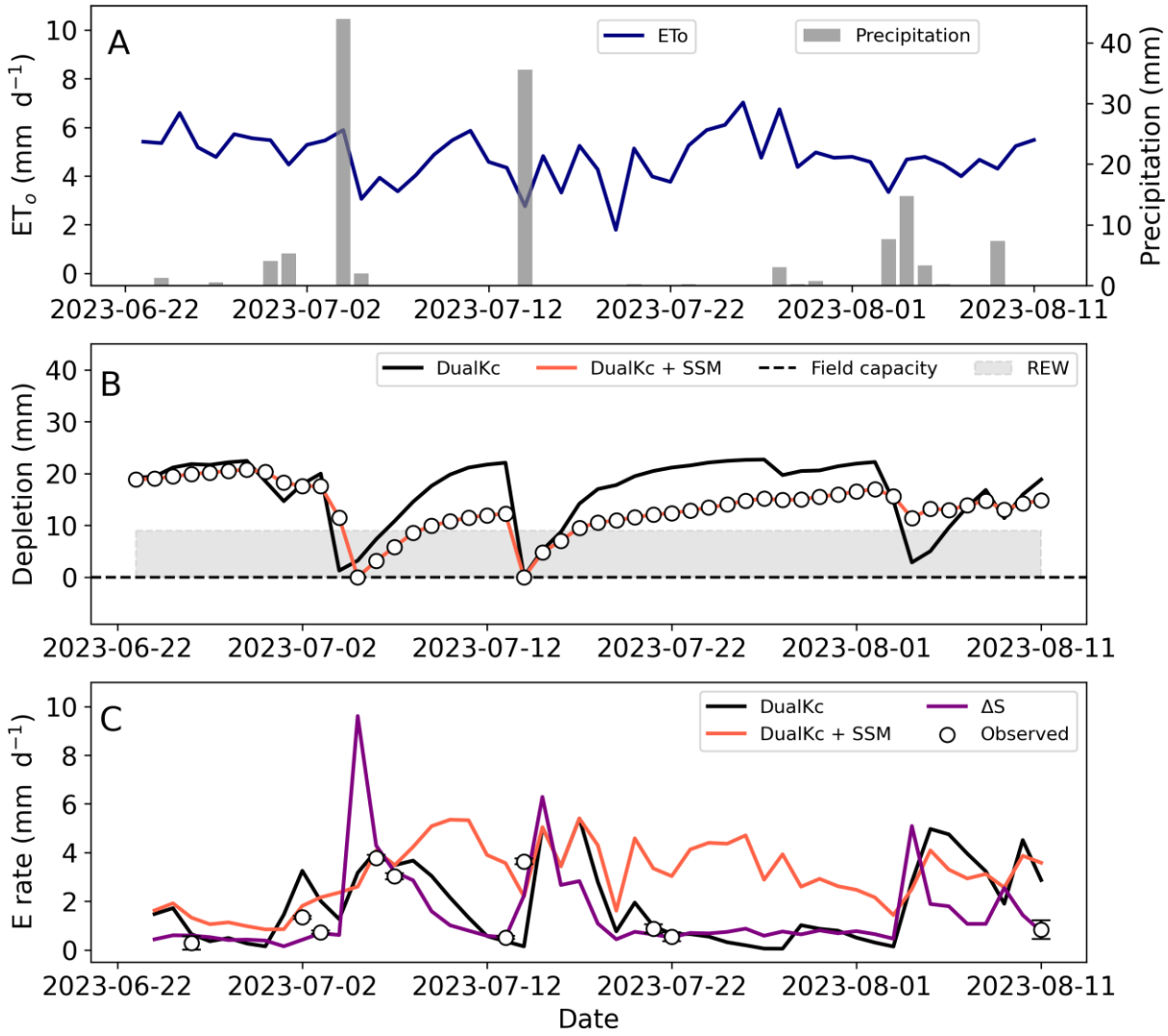

Figure 3-4 (A) Daily reference evapotranspiration (ET_o) and precipitation obtained from the Ashland Bottoms station of the Kansas Mesonet for bare soil summer 2023. (B) Depletion estimated by DualKc and DualKc assimilating surface soil moisture (DualKc + SSM) and the observed values of SSM, the grey bar represents the ready evaporable water (REW) and the black line the field capacity (FC). (C) Soil evaporation rate predicted with the DualKc, DualKc + SSM and the ΔS approach, and *in situ* soil evaporation rate represented with white dots.

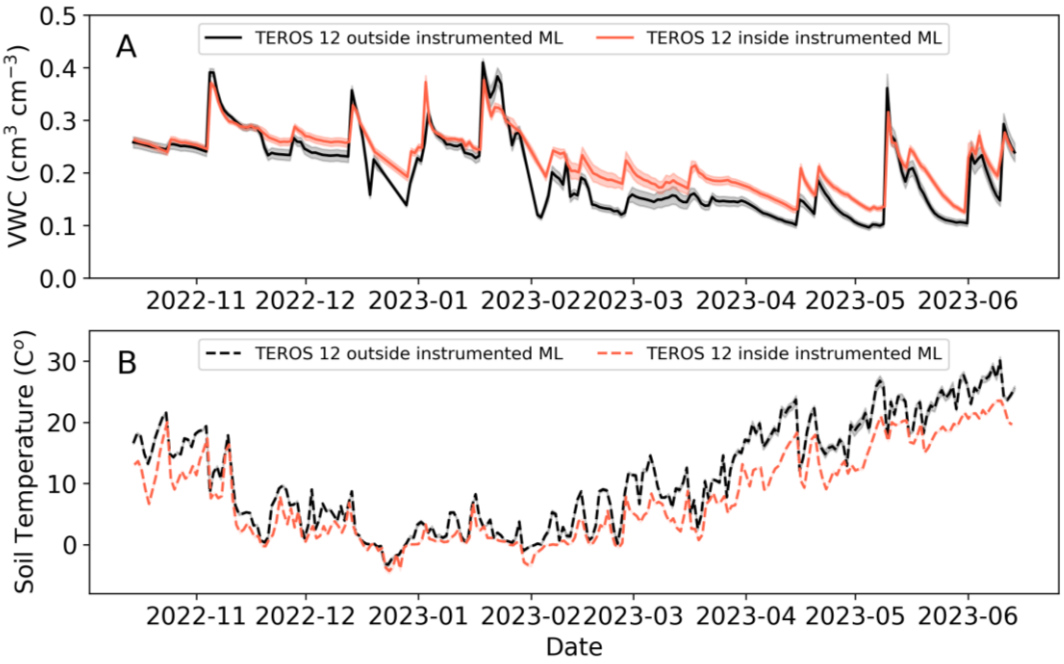

Figure 3-5 (A) Observed volumetric water content (VWC) and (B) observed soil temperature with TEROS 12 inside the microlysimeter (ML) and TEROS 12 outside the microlysimeter during winter wheat growing season 2022/2023.

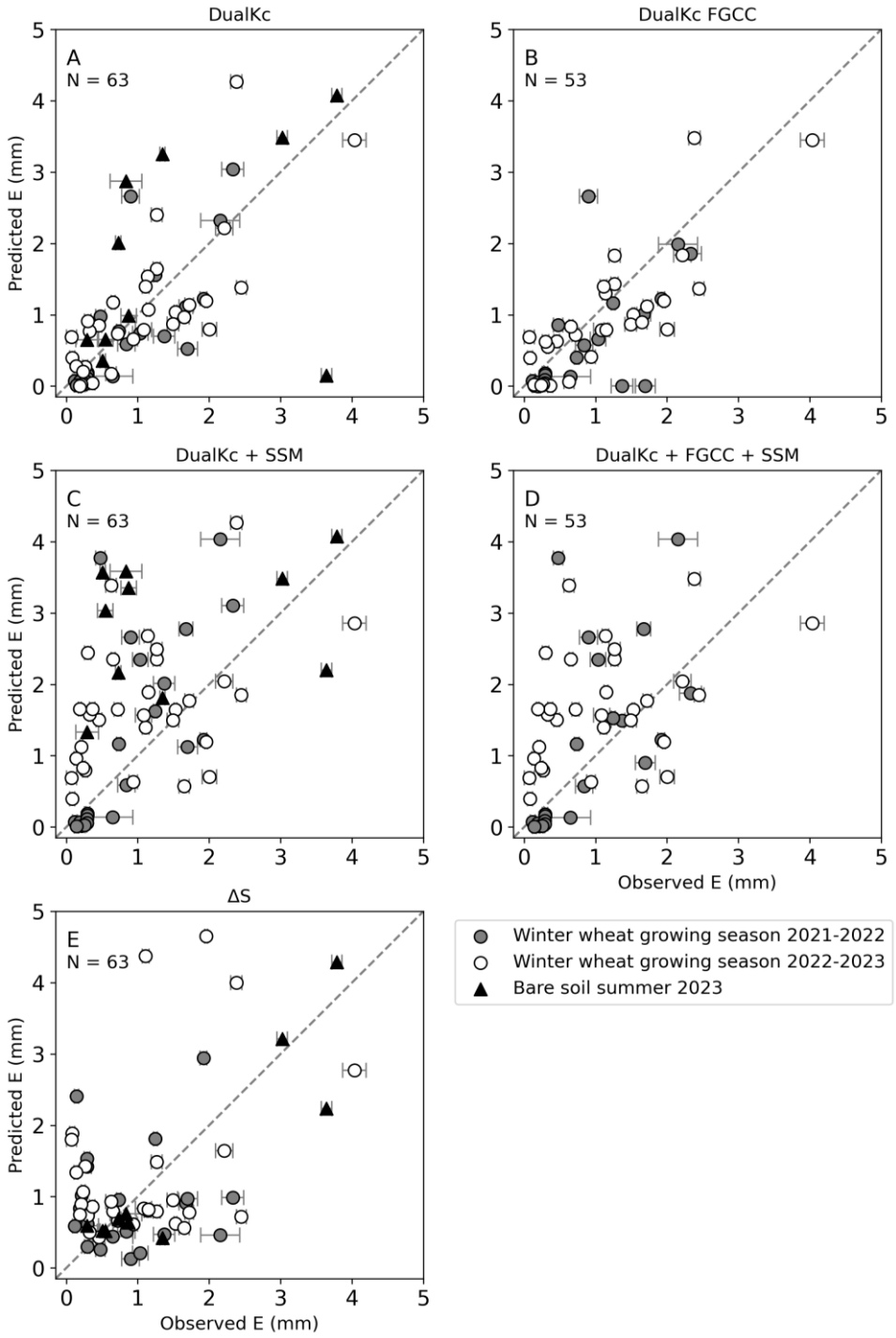

Figure 3-6 Observed evaporation measured with traditional microlysimeter and evaporation estimated with different approaches. (A) DualKc alone, (B) DualKc assimilating fraction of green canopy cover (DualKc + FGCC), (C) DualKc assimilating surface soil moisture (DualKc + SSM), (D) DualKc assimilating FGCC and SSM (DualKc + FGCC + SSM), and (E) Change in storage approach (ΔS).

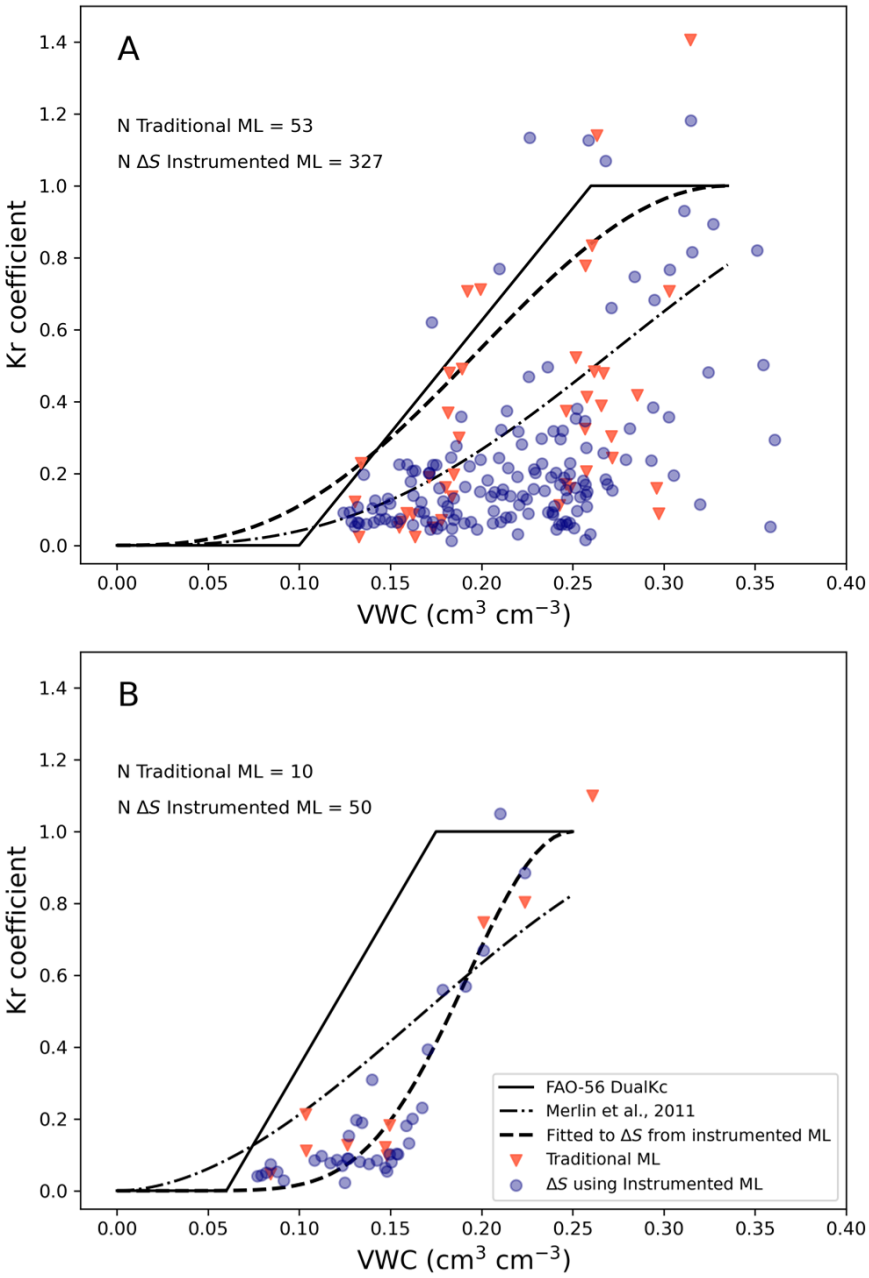

Figure 3-7. Non-linear soil evaporation reduction factor (K_r) for two winter wheat seasons (A) and bare soil (B) fitted with changes in soil water storage (ΔS) from instrumented microlysimeter (ML), traditional ML observations, DualKc regression line and non-linear soil evaporation reduction factor based on soil texture proposed by Merlin et al. (2011).

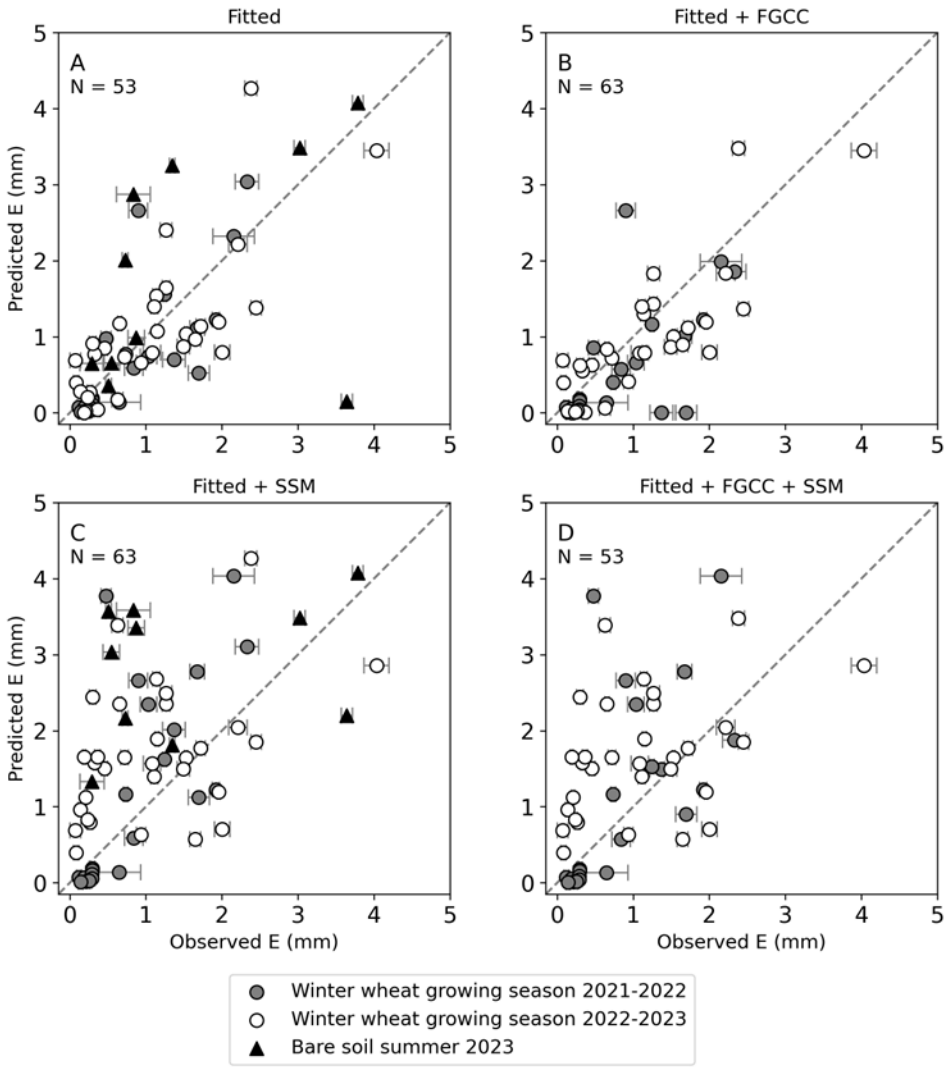

Figure 3-8 Observed soil evaporation measured with traditional microlysimeter and soil evaporation estimated with different approaches. (A) *Fitted* alone, (B) *Fitted* assimilating fraction of green canopy cover (*Fitted* + FGCC), (C) *Fitted* assimilating surface soil moisture (*Fitted* + SSM), (D) *Fitted* assimilating FGCC and SSM (DualKc + FGCC + SSM). N: number of *observations* for each approach.

Chapter 4 - General Conclusions

The soil evaporation process represents a crucial component of the soil water balance, which is characterized by the transfer of water vapor from the soil surface back to the atmosphere. Although some estimations of soil evaporation in the U.S. Great Plains range between 30% to 50%, accurate quantification of soil evaporation remains challenging. Numerous techniques for *in situ* soil evaporation measurements have been developed, as well as computational models to estimate soil evaporation rates. Each of these methods offers advantages and disadvantages, contributing to the complexity of soil evaporation assessment. However, a simple technique for quantifying *in situ* soil evaporation is missing. In response to this research gap, the objective of this study was to integrate *in situ* observations with a model capable of providing daily estimates of the soil evaporation rate.

In the first study, we tested the accuracy and soil sensing volume of two capacitance soil moisture sensors of the TEROS family of sensors. For the TEROS 10 sensor, the cubic polynomial calibration equation with both factory parameters showed root mean square error (RMSE) = 0.027 $cm^3\ cm^{-3}$ and $R^2 = 0.97$, and with fitted parameters RMSE = 0.017 $cm^3\ cm^{-3}$ and $R^2 = 0.99$. For the TEROS 12, the suggested linear calibration model with factory parameters resulted in RMSE = 0.037 $cm^3\ cm^{-3}$ and $R^2 = 0.94$, and with fitted parameters in RMSE = 0.35 $cm^3\ cm^{-3}$ and $R^2 = 0.94$. By adopting a cubic polynomial equation to convert the raw voltage output from the sensor into volumetric water content, we reduce the RMSE = 0.025 $cm^3\ cm^{-3}$, leading to a more accurate estimation of soil moisture ($R^2 = 0.97$). The average sensing volume in dry and moist sand for the TEROS 10 was 288 cm^3, which is 33% lower than the manufacturer-reported values in water. In the case of TEROS 12, the soil sensing volume was 415 cm^3, which is 60% lower than the manufacturer's reported value in water. Further

calibrations should be undertaken to examine the impact of soil temperature and bulk electrical conductivity on the estimation of soil moisture content.

In the second study, our objective was to quantify *in situ* soil evaporation using a model-data assimilation approach in rainfed winter wheat and bare soil. Building upon the accuracy of the capacitance sensor, we developed an instrumented microlysimeter. Surface soil moisture (SSM) observations from the *in situ* sensor were combined with the Dual Crop Coefficient model (DualKc) using a direct insertion method. The three tested data-driven approaches were: DualKc + SSM for both winter wheat and bare soil, DualKc + FGCC + SSM for winter wheat, and the use of the change in surface (top 12 cm) soil water storage (ΔS) for both winter wheat and bare soil. A fourth approach was the DualKc + FGCC for winter wheat, and it yielded the most accurate estimations of daily surface soil evaporation rate in winter wheat, with an average RMSE of 0.604 mm day^{-1} for both seasons. Our findings suggest that improving the partitioning of available energy at the soil surface is crucial for achieving accurate estimations of soil evaporation. Consequently, there is an opportunity to enhance the assessment of canopy cover through *in situ* downward-facing images and high-resolution remote sensing imagery to integrate crop and surface dynamics into empirical and mechanistic models. Contrary to our initial expectations, estimating soil evaporation rate based on ΔS using an open-bottom instrumented microlysimeter produced reasonable estimates of soil evaporation rate for bare soil conditions. Combining this technique with soil hydraulic properties and more advanced numerical models such as HYDRUS or the concept of surface evaporative capacitance could harmonize multiple sources of *in situ* information into a new data-driven technique for *in situ* soil evaporation measurements.

Appendix A - TEROS 10 and TEROS 12 sensor calibration

Appendix A Figure A- 2 Calibration of TEROS 12 with dry (0 cm^3 cm^{-3}) silty clay loam soil in a bucket of 4,000 cm^3.

Appendix B - Model data assimilation approach

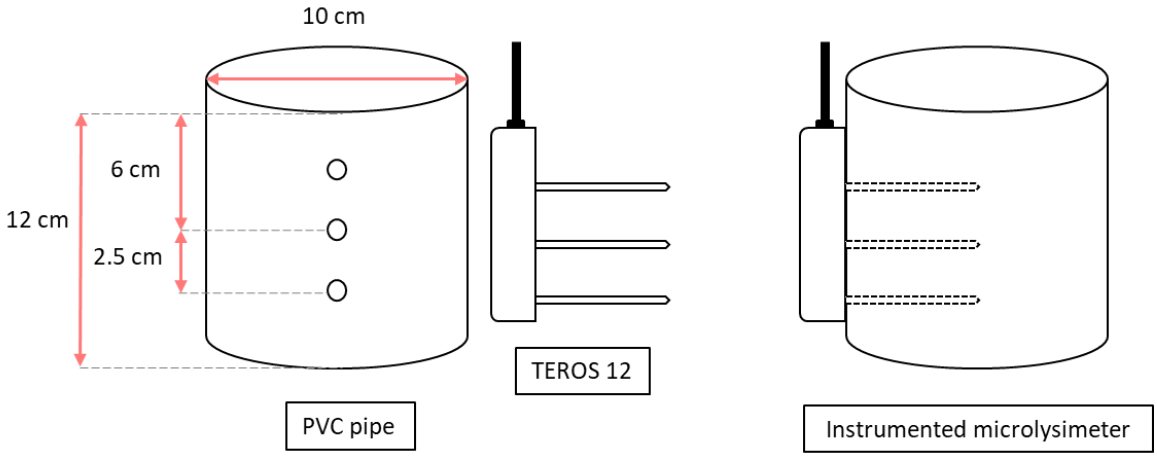

Appendix B Figure B- 2 Instrumented microlysimeter setting.

Dual Crop Coefficient (DualKc) model

$$E = ET_o\ K_r\ (K_{c\,max} - K_{cb})$$

$$K_r = \frac{TEW - D_{e,\,t-1}}{TEW - REW}, \quad \text{for } D_{e,\,t-1} > REW$$

$$D_{e,\,t} = D_{e,\,t-1} - P_t + RO_t + \frac{E_t}{f_{ew,\,t}} + DPe_{,\,t}$$

DualKc + SSM

$$E = ET_o\ K_r\ (K_{c\,max} - K_{cb})$$

$$K_r = \frac{TEW - D_{e,\,t-1}}{TEW - REW}, \quad \text{for } D_{e,\,t-1} > REW$$

$$D_{e,\,t} = TEW - \theta_{sensor,\,t}\ Z_e - 0.5\ \theta_{wp}\ Z_e$$

DualKc Data-driven approach

$$E = ET_o\ K_r\ (K_{c\,max} - K_{cb})$$

$$K_r = \left[0.5 - 0.5\cos\left(\pi \frac{\theta_{sensor,\,t}}{\theta_{FC}}\right)\right]^{\beta}$$

Appendix B Figure B- 3 Reference evapotranspiration (ET_o), reduction coefficient (K_r), maximum value of crop coefficient ($K_{c\,max}$), basal crop coefficient (K_{cb}), depletion (D_e), total evaporable water (TEW), readily evaporable water (REW), precipitation (P), runoff (RO), evaporation (E), fraction of wetted an exposed soil (f_{ew}), deep percolation (DP_e), volumetric water content at field capacity ($\boldsymbol{\theta}_{FC}$)($cm^3\ cm^{-3}$), volumetric water content at wilting point ($\boldsymbol{\theta}_{WP}$), evaporation layer and microlysimeter length (Z_e), curve fitting parameter ($\boldsymbol{\beta}$).

Appendix B Figure B- 4 TEROS 12 soil moisture sensor placed outside the instrumented microlysimeter within the row crop, with surface roots surrounding the sensor rods.